Model-independent bounds probing on the electromagnetic dipole moments of the τ-lepton at the CLIC

M. Köksal[*],[1] A. A. Billur[†],[2] A. Gutiérrez-Rodríguez[‡],[3] and M. A. Hernández-Ruíz[§][4]

[1]Deparment of Optical Engineering, Cumhuriyet University, 58140, Sivas, Turkey.

[2]Deparment of Physics, Cumhuriyet University, 58140, Sivas, Turkey.

[3]Facultad de Física, Universidad Autónoma de Zacatecas

Apartado Postal C-580, 98060 Zacatecas, México.

[4]Unidad Académica de Ciencias Químicas, Universidad Autónoma de Zacatecas

Apartado Postal C-585, 98060 Zacatecas, México.

(Dated: April 9, 2018)

Abstract

We establish model independent bounds on the anomalous magnetic and electric dipole moments of the tau-lepton using the two-photon processes $\gamma\gamma \to \tau^+\tau^-$ and $\gamma\gamma \to \tau^+\tau^-\gamma$. We use $\mathcal{L} = 10, 50, 100, 300, 500, 1000, 1500, 2000, 3000 \ fb^{-1}$ of data collected with the future e^+e^- linear collider such as the CLIC at $\sqrt{s} = 380, 1500, 3000 \ GeV$ and we consider systematic uncertainties of $\delta_{sys} = 0, 3, 5 \ \%$. Precise bounds at 95% C. L. on the anomalous dipole moments to the tau-lepton $-0.00015 \le \tilde{a}_\tau \le 0.00017$ and $|\tilde{d}_\tau(ecm)| = 9.040 \times 10^{-19}$ are set from our study. Our results show that the processes under consideration are a very good prospect for probing the dipole moments of the tau-lepton at the future e^+e^- linear collider at the $\gamma\gamma$ mode.

[*] mkoksal@cumhuriyet.edu.tr

[†] abillur@cumhuriyet.edu.tr

[‡] alexgu@fisica.uaz.edu.mx

[§] mahernan@uaz.edu.mx

1

I. INTRODUCTION

One of the greatest achievement of the Standard Model (SM) [1–3] is the measurement of the electric (EDM) and magnetic (MM) dipole moments of the electron and muon $g-2$, which have been measured with a excellent precision of

$$a_e^{Exp} = 1159652180.73(28) \times 10^{-12} \qquad [0.24\,\text{ppb}] \quad [4], \tag{1}$$

$$a_\mu^{Exp} = 11659209.1(5.4)(3.3) \times 10^{-10} \qquad [0.54\,\text{ppm}] \quad [5], \tag{2}$$

respectively, and the theoretical prediction of the SM [6] is given by

$$a_\mu^{SM} = 116591803(1)(42)(26) \times 10^{-11}. \tag{3}$$

On the other hand, in comparison with the electron or muon mass, the tau-lepton has a large mass of $m_\tau = 1776.82 \pm 0.16\,MeV$ [6], allowing one to expected an essential enhancement in the sensitivity to the effects of new physics beyond the Standard Model (BSM), such as its dipole moments [7]. However the very short lifetime of this unstable particle makes it impossible to directly measure their electromagnetic properties. Therefore, indirect information must be obtained by precisely measuring cross sections and decay rates in processes involving the emission of a real photon by the tau-lepton.

With respect to the anomalous magnetic moment of the τ-lepton, the SM prediction is $a_\tau^{SM} = 117721(5) \times 10^{-8}$ [8, 9] and the respective EDM d_τ is generated by the GIM mechanism only at very high order in the coupling constant [10]. The error with an order of magnitude of 10^{-8} is an indication that SM extensions predicting values for a_τ above this level they are worth studying, as well as it is worthwhile to study new mechanisms and new modes of production of tau pairs in association with a photon $\tau^+\tau^-\gamma$ at the future e^+e^- linear collider at the $\gamma\gamma$ mode.

The SM predicts CP violation, which is necessary for the existence of the EDM of a variety physical systems. The EDM provides a direct experimental probe of CP violation [11–13], a feature of the SM and BSM physics. Precise measurement of the EDM of fundamental charged particles provides a significant probe of physics BSM.

The sensitivity to the MM and EDM of the tau-lepton has been studied in different context, both theoretical and experimental and some of which are summarized in Table I.

TABLE I: Summary of experimental and theoretical limits on the electromagnetic dipole moments of the tau-lepton.

Collaboration	Experimental limit	C. L.	Reference
DELPHI	$-0.052 < a_\tau < 0.013$	95%	[14]
L3	$-0.052 < a_\tau < 0.058$	95%	[15]
OPAL	$-0.068 < a_\tau < 0.065$	95%	[16]
Collaboration	Experimental limit	C. L.	Reference
BELLE	$-2.2 < Re(d_\tau(10^{-17}ecm)) < 4.5$	95%	[17]
	$-2.5 < Im(d_\tau(10^{-17}ecm)) < 0.8$	95%	
DELPHI	$-0.22 < d_\tau(10^{-16}ecm) < 0.45$	95%	[14]
L3	$|Re(d_\tau(10^{-16}ecm))| < 3.1$	95%	[15]
OPAL	$|Re(d_\tau(10^{-16}ecm))| < 3.7$	95%	[16]
ARGUS	$|Re(d_\tau(10^{-16}ecm))| < 4.6$	95%	[18]
	$|Im(d_\tau(10^{-16}ecm))| < 1.8$	95%	
Model	Theoretical limit	C. L.	Reference
L3 data	$a_\tau \leq 0.11$	90%	[19]
Electroweak Measurements	$-0.004 < a_\tau < 0.006$	95%	[20]
LEP1, SLC, LEP2 Data	$-0.007 < a_\tau < 0.005$	95%	[21]
Total cross section	$a_\tau < 0.023$	95%	[22]
Model	Theoretical limit	C. L.	Reference
L3 data	$d_\tau \leq 6 \times 10^{-16}ecm$	90%	[19]
Electroweak Measurements	$d_\tau \leq 1.1 \times 10^{-17}ecm$	95%	[20]
Cross section	$d_\tau \leq 1.6 \times 10^{-16}ecm$	90%	[23]

Furthermore, there is an extensive theoretical work done in models BSM that contribute to dipole moments of charged leptons: Extra dimensions [24], Seesaw model [25], version III of the 2HDM [26], Non-commutative geometry [27], Non-universal extra dimensions [28], Left-Right symmetric model [29], E_6 Superstring models [30], Simplest little Higgs model [31], 331 model [32]. There are also bounds independent of the model such as γp collisions

[33], $e^-\gamma$ scattering [34] and $\gamma\gamma$ collisions [35, 36]. Other limits on the MM and EDM of the τ-lepton are reported in Refs. [7, 37–50].

In this paper, using $\gamma\gamma \to \tau^+\tau^-$ and $\gamma\gamma \to \tau^+\tau^-\gamma$ reactions, we establish model independent limits on the dipole moments of the tau-lepton, and we improve the existing bounds on a_τ and d_τ. An interesting feature of these reactions is that they are extremely clean process because it has not interference with weak interactions, being a purely process of Quantum Electrodynamics (QED). Furthermore, the high center-of-mass energies proposed for the Compact Linear Collider (CLIC) make of it an appropriate machine to probing the MM and EDM which are more sensitive with the high energy and high luminosity of the collider.

The CLIC [51–54] is a proposal for a future e^+e^- linear collider at CERN in the High Luminosity-Large Hadron Collider (HL-LHC) era. The machine is designed to make full use of the physics potential of CLIC with initial operation at center-of-mass energy of $\sqrt{s} = 380\,GeV$ and luminosity of $\mathcal{L} = 500\,fb^{-1}$. The following stages at center-of-mass energies of $\sqrt{s} = 1500\,GeV$ ($\mathcal{L} = 1500\,fb^{-1}$) and $\sqrt{s} = 3000\,GeV$ ($\mathcal{L} = 3000\,fb^{-1}$) focus on exploring physics BSM. In summary, the CLIC project offers a rich physics program for about 20 years, with discovery potential to new physics, that can reach scales of up to several tens of TeV, through indirect searches with precision measurements.

For our study, we consider the following parameters of the CLIC: $\sqrt{s} = 380, 1500, 3000\,GeV$, $\mathcal{L} = 10, 50, 100, 300, 500, 1000, 1500, 2000, 3000\,fb^{-1}$ and we consider systematic uncertainties of $\delta_{sys} = 0, 3, 5\,\%$, with these parameters as input, we established model independent bounds on the electromagnetic dipole moments of the τ-lepton at 95% C.L.. We get stringent limits in comparison with the bounds obtained by the DELPHI, L3, OPAL, BELLE and ARGUS Collaborations [14–18] (see Table I).

The remainder of the paper is organized as follows: In Section II, we study the total cross section and the electromagnetic dipole moments of the tau-lepton through the $\gamma\gamma \to \tau^+\tau^-$ and $\gamma\gamma \to \tau^+\tau^-\gamma$ reactions. Section III provides the conclusions.

II.   TWO-PHOTON PROCESSES $\gamma\gamma \to \tau^+\tau^-$ AND $\gamma\gamma \to \tau^+\tau^-\gamma$

For our study, we will take advantage of our previous works on the collision modes $\gamma\gamma$, $\gamma\gamma^*$ and $\gamma^*\gamma^*$ [35, 55–57] for calculate the total cross section for the $\gamma\gamma \to \tau^+\tau^-$ and $\gamma\gamma \to \tau^+\tau^-\gamma$

reactions. The corresponding Feynman diagrams for these processes are given in Figs. 1 and 2, respectively.

In our study we deduce bounds on the electromagnetic dipole moments of the τ-lepton a_τ and d_τ via the two-photon processes $\gamma\gamma \to \tau^+\tau^-$ and $\gamma\gamma \to \tau^+\tau^-\gamma$. These processes are of interest for a number of reasons: First, are sensitive to the a_τ and d_τ. Additionally, increased cross sections for high energies and the absence or stong suppression of weak contributions are further complementary aspects of the two-photon processes in the contrast with the direct processes $e^+e^- \to \tau^+\tau^-$ [18, 23], $e^+e^- \to \tau^+\tau^-\gamma$ [15] and $Z \to \tau^+\tau^-\gamma$ [16, 19]. Furthermore, an important point is the availability of high luminosity photon beams due to Bremsstrahlung as a byproduct in planned high energy colliders. Also, very hard photons at high luminosity may be produced in Compton backscattering of laser light off high energy e^+e^- beams, as is the case of the future CLIC.

In order to determine the bounds on the MM and EDM of the τ-lepton, we calculate the total cross section of the reactions $\gamma\gamma \to \tau^+\tau^-$ and $\gamma\gamma \to \tau^+\tau^-\gamma$. The most general parametrization for the electromagnetic current between on-shell tau-lepton and the photon is given by [7, 19, 20, 58]

$$\Gamma_\tau^\alpha = eF_1(q^2)\gamma^\alpha + \frac{ie}{2m_\tau}F_2(q^2)\sigma^{\alpha\mu}q_\mu + \frac{e}{2m_\tau}F_3(q^2)\sigma^{\alpha\mu}q_\mu\gamma_5 + eF_4(q^2)\gamma_5(\gamma^\alpha - \frac{2q^\alpha m_\tau}{q^2}), \quad (4)$$

where e is the charge of the electron, m_τ is the mass of the tau-lepton, $\sigma^{\alpha\mu} = \frac{i}{2}[\gamma^\alpha, \gamma^\mu]$ represents the spin 1/2 angular momentum tensor and $q = p' - p$ is the momentum transfer. In the static (classical) limit the q^2-dependent form factors $F_{1,2,3,4}(q^2)$ have familiar interpretations for $q^2 = 0$: $F_1(0) = Q_\tau$ is the electric charge; $F_2(0) = a_\tau$ its anomalous MM and $F_3(0) = \frac{2m_\tau}{e}d_\tau$ with d_τ its EDM. $F_4(q^2)$ is the Anapole form factor.

In phenomenological and experimental searches most of the tau-lepton electromagnetic vertices search involve off-shell tau-leptons. Indeed in these studies one of the tau-lepton is off-shell and measured quantity is not directly a_τ and d_τ. For this reason deviations of the tau-lepton dipole moments from the SM values are examined in an effective lagrangian approach. It is usually common to study new physics in a model independent way through the effective lagrangian approach. This approach is defined by high-dimensional operators which lead to anomalous $\tau^+\tau^-\gamma$ coupling. In this study, we will apply the dimension-six effective operators that contribute to the electric and magnetic dipole moments of the tau-

lepton at the tree level given by Ref. [59–61]:

$$L_{eff} = \frac{1}{\Lambda^2}\left[C_{LW}^{33}Q_{LW}^{33} + C_{LB}^{33}Q_{LB}^{33}\right], \tag{5}$$

where

$$Q_{LW}^{33} = \left(\bar{\ell}_\tau\sigma^{\mu\nu}\tau_R\right)\sigma^I\varphi W_{\mu\nu}^I, \tag{6}$$

$$Q_{LB}^{33} = \left(\bar{\ell}_\tau\sigma^{\mu\nu}\tau_R\right)\varphi B_{\mu\nu}. \tag{7}$$

Here, φ and ℓ_τ are the Higgs and the left-handed $SU(2)$ doublets, σ^I are the Pauli matrices and $W_{\mu\nu}^I$ and $B_{\mu\nu}$ are the gauge field strength tensors.

After the electroweak symmetry breaking from the effective lagrangian in Eq. (5), the CP even κ and CP odd $\tilde{\kappa}$ parameters are obtained

$$\kappa = \frac{2m_\tau}{e}\frac{\sqrt{2}\upsilon}{\Lambda^2}Re\left[\cos\theta_W C_{LB}^{33} - \sin\theta_W C_{LW}^{33}\right], \tag{8}$$

$$\tilde{\kappa} = \frac{2m_\tau}{e}\frac{\sqrt{2}\upsilon}{\Lambda^2}Im\left[\cos\theta_W C_{LB}^{33} - \sin\theta_W C_{LW}^{33}\right], \tag{9}$$

where $\upsilon = 246$ GeV and $\sin\theta_W$ is the weak mixing angle.

These parameters are related to contribution of the anomalous magnetic and electric dipole moments of the tau-lepton through the following relations:

$$\kappa = \tilde{a}_\tau, \tag{10}$$

$$\tilde{\kappa} = \frac{2m_\tau}{e}\tilde{d}_\tau. \tag{11}$$

A. $\gamma\gamma \to \tau^+\tau^-$ cross section

All signal cross sections in this paper are computed using the package CALCHEP 3.6.30 [62], which can computate the Feynman diagrams, integrate over multiparticle phase space and event simulation. In addition, for our study we consider the following basic acceptance cuts for $\tau^+\tau^-$ events at the CLIC:

$$p_t^{\tau,\bar{\tau}} > 20\,GeV,$$
$$|\eta^{\tau,\bar{\tau}}| < 2.5, \tag{12}$$
$$\Delta R(\tau,\bar{\tau}) > 0.4,$$

we apply these cuts to reduce the background and to optimize the signal sensitivity. In Eq. (12), $p_t^{\tau,\bar{\tau}}$ is the transverse momentum of the final state particles, $\eta^{\tau,\bar{\tau}}$ is the pseudorapidity which reduces the contamination from other particles misidentified as tau and $\Delta R(\tau,\bar{\tau})$ is the separation of the final state particles.

The tau-lepton was discovered by Martin Lewis Perl in 1975 [63, 64]. It was discovered in the Stanford Positron and Electron Accelerator Ring (SPEAR) of SLAC with the MARK I detector. With these tools, Perl and his team managed to distinguish leptons, hadrons and photons fairly accurately. The tau-lepton was discovered from certain anomalies detected in the disintegration of the particles. The observed event was as follows

$$e^+e^- \to \tau^+\tau^- \to e^\pm + \mu^\pm + \nu_e + \bar{\nu}_\mu + \nu_\tau + \bar{\nu}_\tau.$$

When making the energy balance between the initial and final states, it was observed that the final energy was lower. At no time did the muons, hadrons and photons sum the energy necessary to equal the initial state. Then it was thought that the energy that made the electron and the positron collider created a pair of new particles very massive, which soon decay into the other observed particles. This theory was difficult to verify because the energy needed to produce the tau-antitau pair was similar to that required to create a pair of mesons. Subsequent experiments carried out in DESY and in SLAC confirmed the existence of the tau lepton and provided more precise values for its mass and spin.

The tau is the only lepton that has the mass necessary to disintegrate, most of the time in hadrons. 17.8% of the time the tau decays into an electron and into two neutrinos; in another 17.4% of the time, it decays in a muon and in two neutrinos. In the remaining

64.8% of the occasions, it decays in the form of hadrons and a neutrino. In Table II the main τ-decay branching ratios are shown.

TABLE II: The main τ-decay branching ratios [6, 65].

Channel	Branching Ratios (%)
$\tau \to e^- \nu_e \nu_\tau$	17.8
$\tau \to \mu \nu_\mu \nu_\tau$	17.4
$\tau \to \pi^\pm \nu_\tau$	11.1
$\tau \to \pi^0 \pi^\pm \nu_\tau$	25.4
$\tau \to \pi^0 \pi^0 \pi^\pm \nu_\tau$	9.19
$\tau \to \pi^0 \pi^0 \pi^0 \pi^\pm \nu_\tau$	1.08
$\tau \to \pi^\pm \pi^\pm \pi^\pm \nu_\tau$	8.98
$\tau \to \pi^0 \pi^\pm \pi^\pm \pi^\pm \nu_\tau$	4.30
$\tau \to \pi^0 \pi^0 \pi^\pm \pi^\pm \pi^\pm \nu_\tau$	0.50
$\tau \to \pi^0 \pi^0 \pi^0 \pi^\pm \pi^\pm \pi^\pm \nu_\tau$	0.11
$\tau \to K^\pm X \nu_\tau$	3.74
$\tau \to (\pi^0) \pi^\pm \pi^\pm \pi^\pm \pi^\pm \pi^\pm \nu_\tau$	0.10
Others	0.03

Since its discovery in 1975, the lepton-tau has been important to check different aspects of the SM. In particular, since the tau is the charged lepton of the third generation, the verification of its properties can give light on the problems related to the replication of generations, which is one of the open problems of the SM. Furthermore, it is the heavier lepton which makes it especially more sensitive to new physics, since its coupling to the dynamics responsible for the generation of masses, whatever it is, is more intense. In addition, it is the only lepton heavy enough to disintegrate into hadrons, which makes this particle a particularly suitable system for studying Quantum Chromodynamics (QCD) at low energies.

The square matrix elements for the process $\gamma\gamma \to \tau^+ \tau^-$ as a function of the Mandelstam invariants $\hat{s}$, $\hat{t}$ and $\hat{u}$ are given by:

$$|M_1|^2 = \frac{16\pi^2 Q_\tau^2 \alpha_e^2}{2m_\tau^4(\hat{t}-m_\tau^2)^2}\left[48\kappa(m_\tau^2-\hat{t})(m_\tau^2+\hat{s}-\hat{t})m_\tau^4 - 16(3m_\tau^4-m_\tau^2\hat{s}+\hat{t}(\hat{s}+\hat{t}))m_\tau^4 \right.$$
$$+ 2(m_\tau^2-\hat{t})(\kappa^2(17m_\tau^4+(22\hat{s}-26\hat{t})m_\tau^2+\hat{t}(9\hat{t}-4\hat{s}))$$
$$+ \tilde{\kappa}^2(17m_\tau^2+4\hat{s}-9\hat{t})(m_\tau^2-\hat{t}))m_\tau^2 + 12\kappa(\kappa^2+\tilde{\kappa}^2)\hat{s}(m_\tau^3-m_\tau\hat{t})^2$$
$$\left. - (\kappa^2+\tilde{\kappa}^2)^2(m_\tau^2-\hat{t})^3(m_\tau^2-\hat{s}-\hat{t})\right], \tag{13}$$

$$|M_2|^2 = \frac{-16\pi^2 Q_\tau^2 \alpha_e^2}{2m_\tau^4(\hat{u}-m_\tau^2)^2}\left[48\kappa(m_\tau^4+(\hat{s}-2\hat{t})m_\tau^2+\hat{t}(\hat{s}+\hat{t}))m_\tau^4 \right.$$
$$+ 16(7m_\tau^4-(3\hat{s}+4\hat{t})m_\tau^2+\hat{t}(\hat{s}+\hat{t}))m_\tau^4$$
$$+ 2(m_\tau^2-\hat{t})(\kappa^2(m_\tau^4+(17\hat{s}-10\hat{t})m_\tau^2+9\hat{t}(\hat{s}+\hat{t}))$$
$$+ \tilde{\kappa}^2(m_\tau^2-9\hat{t})(m_\tau^2-\hat{t}-\hat{s}))m_\tau^2$$
$$\left. + (\kappa^2+\tilde{\kappa}^2)^2(m_\tau^2-\hat{t})^3(m_\tau^2-\hat{s}-\hat{t})\right], \tag{14}$$

$$M_1^\dagger M_2 + M_2^\dagger M_1 = \frac{16\pi^2 Q_\tau^2 \alpha_e^2}{m_\tau^2(\hat{t}-m_\tau^2)(\hat{u}-m_\tau^2)}$$
$$\times \left[-16(4m_\tau^6-m_\tau^4\hat{s})+8\kappa m_\tau^2(6m_\tau^4-6m_\tau^2(\hat{s}+2\hat{t})-\hat{s})^2\right.$$
$$+ 6\hat{t})^2+6\hat{s}\hat{t})+(\kappa^2(16m_\tau^6-m_\tau^4(15\hat{s}+32\hat{t})+m_\tau^2(15\hat{s})^2$$
$$+ 14\hat{t}\hat{s}+16\hat{t})^2)+\hat{s}\hat{t}(\hat{s}+\hat{t}))+\tilde{\kappa}^2(16m_\tau^6-m_\tau^4(15\hat{s}+32\hat{t})$$
$$+ m_\tau^2(5\hat{s})^2+14\hat{t}\hat{s}+16\hat{t})^2)+\hat{s}\hat{t}(\hat{s}+\hat{t})))-4\kappa\hat{s}(\kappa^2+\tilde{\kappa}^2)$$
$$\times (m_\tau^4+m_\tau^2(\hat{s}-2\hat{t})+\hat{t}(\hat{s}+\hat{t}))-4\tilde{\kappa}(\kappa^2+\tilde{\kappa}^2)(2m_\tau^2-\hat{s}-2\hat{t})$$
$$\left.\times \epsilon_{\alpha\beta\gamma\delta}p_1^\alpha p_2^\beta p_3^\gamma p_4^\delta - 2\hat{s}(\kappa^2+\tilde{\kappa}^2)^2(m_\tau^4-2\hat{t}m_\tau^2+\hat{t}(\hat{s}+\hat{t}))\right], \tag{15}$$

where $\hat{s}=(p_1+p_2)^2=(p_3+p_4)^2$, $\hat{t}=(p_1-p_3)^2=(p_4-p_2)^2$, $\hat{u}=(p_3-p_2)^2=(p_1-p_4)^2$, and p_1 and p_2 are the four-momenta of the incoming photons, p_3 and p_4 are the momenta of the outgoing tau-lepton, Q_τ is the tau-lepton charge, α_e is the fine-structure constant and m_τ is the mass of the tau.

The most promising mechanism to generate energetic photon beams in a linear collider is Compton backscattering. Compton backscattered photons interact with each other and generate the process $\gamma\gamma \to \tau^+\tau^-$. The spectrum of Compton backscattered photons is given by

$$f_\gamma(y) = \frac{1}{g(\zeta)}[1 - y + \frac{1}{1 - y} - \frac{4y}{\zeta(1 - y)} + \frac{4y^2}{\zeta^2(1 - y)^2}], \tag{16}$$

where

$$g(\zeta) = (1 - \frac{4}{\zeta} - \frac{8}{\zeta^2}) \log{(\zeta + 1)} + \frac{1}{2} + \frac{8}{\zeta} - \frac{1}{2(\zeta + 1)^2}, \tag{17}$$

with

$$y = \frac{E_\gamma}{E_e}, \quad \zeta = \frac{4E_0 E_e}{M_e^2}, \quad y_{max} = \frac{\zeta}{1 + \zeta}. \tag{18}$$

Here, E_0 and E_e are energy of the incoming laser photon and initial energy of the electron beam before Compton backscattering and E_γ is the energy of the backscattered photon. The maximum value of y reaches 0.83 when $\zeta = 4.8$.

The total cross section is given by,

$$\sigma = \int f_\gamma(x) f_\gamma(x) d\hat{\sigma} dE_1 dE_2. \tag{19}$$

Next, we present the total cross section as a polynomial in powers of $\kappa(\tilde{\kappa})$. This provides more precise and convenient information for the study of the process $\gamma\gamma \rightarrow \tau^+\tau^-$. We consider the following cases:

- For $\sqrt{s} = 380\,GeV$.

$$\begin{aligned}
\sigma(\kappa) &= \left[(9.73 \times 10^6)\kappa^4 + (8.18 \times 10^4)\kappa^3 + (8.13 \times 10^4)\kappa^2 + (1.11 \times 10^2)\kappa + 38.75\right](pb), \\
\sigma(\tilde{\kappa}) &= \left[(9.73 \times 10^6)\tilde{\kappa}^4 + (8.26 \times 10^4)\tilde{\kappa}^2 + 38.75\right](pb).
\end{aligned} \tag{20}$$

- For $\sqrt{s} = 1500\,GeV$.

$$\begin{aligned}
\sigma(\kappa) &= \left[(1.54 \times 10^8)\kappa^4 + (8.42 \times 10^8)\kappa^3 + (8.80 \times 10^4)\kappa^2 + (17.5)\kappa + 6\right](pb), \\
\sigma(\tilde{\kappa}) &= \left[(1.54 \times 10^8)\tilde{\kappa}^4 + (8.81 \times 10^4)\tilde{\kappa}^2 + 6\right](pb).
\end{aligned} \tag{21}$$

10

- For $\sqrt{s} = 3000\,GeV$.

$$
\begin{aligned}
\sigma(\kappa) &= \left[(6.17 \times 10^8)\kappa^4 + (9.13 \times 10^4)\kappa^3 + (8.72 \times 10^4)\kappa^2 - (1.21)\kappa + 1.97\right](pb), \\
\sigma(\tilde{\kappa}) &= \left[(6.17 \times 10^8)\tilde{\kappa}^4 + (8.83 \times 10^4)\tilde{\kappa}^2 + 1.97\right](pb).
\end{aligned} \tag{22}
$$

From Eqs. (20)-(22), the linear, quadratic and cubic terms in $\kappa(\tilde{\kappa})$ arise from the interference between SM and anomalous amplitudes, whereas the quartic terms are purely anomalous. The independent term of $\kappa(\tilde{\kappa})$ correspond to the cross section at $\kappa = \tilde{\kappa} = 0$ and represents the contribution of the cross section of the SM.

B. Bounds on the $\tilde{a}_\tau$ and $\tilde{d}_\tau$ through $\gamma\gamma \to \tau^+\tau^-$ at the CLIC

For our numerical analysis of the total cross section $\sigma_{NP}(\gamma\gamma \to \tau^+\tau^-) = \sigma_{NP}(\sqrt{s}, \kappa, \tilde{\kappa})$, as well as of the electromagnetic dipole moments of the tau-lepton, where the free parameters are the center-of-mass energy $\sqrt{s}$, the integrated luminosity $\mathcal{L}$ of the CLIC and the factors κ and $\tilde{\kappa}$, we also consider the acceptance cuts given in Eq. (12). In addition, we take into account the systematic uncertainties for the collider. For this purpose, we use the usual formula for the χ^2 function [33–35, 66]:

$$
\chi^2 = \left(\frac{\sigma_{SM} - \sigma_{NP}(\sqrt{s}, \kappa, \tilde{\kappa})}{\sigma_{SM}\delta}\right)^2, \tag{23}
$$

where $\sigma_{NP}(\sqrt{s}, \kappa, \tilde{\kappa})$ is the total cross section including contributions from the SM and new physics, $\delta = \sqrt{(\delta_{st})^2 + (\delta_{sys})^2}$, $\delta_{st} = \frac{1}{\sqrt{N_{SM}}}$ is the statistical error, δ_{sys} is the systematic error and N_{SM} is the number of signal expected events $N_{SM} = \mathcal{L}_{int} \times BR \times \sigma_{SM}$ where $\mathcal{L}_{int}$ is the integrated CLIC luminosity. Furthermore, as the tau-lepton decays roughly 35% of the time leptonically and 65% of the time to one or more hadrons (see Table II), then for the signal we consider one of the tau-leptons decays leptonically and the other hadronically. Therefore, for our study we assume that the Branching ratio of the two-tau in the final state to be BR=0.46.

Systematic uncertainties may occur when tau-lepton is identified due to some of the reasons described below: Although, we do not have any CLIC reports [67–69] to know exactly what the systematic uncertainties are for our processes which are investigated, we will make some approaches about the systematic uncertainties. The DELPHI Collaboration examined

11

TABLE III: Systematic errors given by the DELPHI Collaboration [14].

	1997	1998	1999	2000
Trigger efficiency	7.0	2.7	3.6	4.5
Selection efficiency	5.1	3.2	3.0	3.0
Background	1.7	0.9	0.9	0.9
Luminosity	0.6	0.6	0.6	0.6
Total	8.9	4.3	4.7	5.4

the anomalous magnetic and electric dipole moments of the tau-lepton through the process $e^+e^- \to e^+e^-\tau^+\tau^-$ in the years $1997 - 2000$ at collision energy $\sqrt{s}$ between 183 and 208 GeV [14]. Relative systematic errors on cross section of the process $e^+e^- \to e^+e^-\tau^+\tau^-$ are given in Table III. Also, the process $e^+e^- \to e^+e^-\tau^+\tau^-$ was studied with the L3 detector for center-of-mass energies 161 GeV$\leqslant \sqrt{s} \leqslant$ 209 GeV at LEP [15]. The anomalous magnetic and electric dipole moments of the tau-lepton via the process $pp \to pp\tau^+\tau^-$ with 2% of the total systematic uncertainties at the LHC was investigated phenomenologically in Ref [70]. Work in this regard is done by ATLAS and CMS groups [65, 71, 72]. Tau tagging efficiencies also studied for the International Large Detector (ILD) [73], a proposed detector concept for the International Linear Collider (ILC). Due to these difficulties, tau identification efficiencies are always calculated for specific process, luminosity, and kinematic parameters. These studies are currently being carried out by various groups for selected productions. For a realistic efficiency, we need a detailed study for our specific process and kinematic parameters. For all these reasons, in this work, kinematic cuts contain some general values chosen by detectors for lepton identification. Hence, in this paper, tau-lepton identification efficiency is considered within systematic errors. Taking into consideration the previous studies, 3% and 5% of total systematic uncertainties were taken in this study. It can be assumed that this accelerator will be built in the coming years and the systematic uncertainties will be lower when considering the development of future detector technology.

With all these elements that we taken into consideration, we made and presented a set of figures, as well as tables which illustrate our results.

The total cross sections $\sigma_{\gamma\gamma \to \tau^+\tau^-}(\sqrt{s}, \kappa, \tilde{\kappa})$ are presented as a function of the anomalous couplings κ in Fig. 3 and $\tilde{\kappa}$ in Fig. 4 for the center-of-mass energies of $\sqrt{s} =$

$380, 1500, 3000\,GeV$, respectively. The total cross section clearly shows a strong dependence with respect to the anomalous parameters κ, $\tilde{\kappa}$ and with the center-of-mass energy of the collider $\sqrt{s}$. Additionally, the $\sigma_{\gamma\gamma\to\tau^+\tau^-}(\sqrt{s},\kappa,\tilde{\kappa})$ as function of κ and $\tilde{\kappa}$ are shown in Figs. 5-7. In these figures, the surfaces are increased for the lower and upper limits of the parameters κ and $\tilde{\kappa}$, showing a strong dependence with respect to these parameters.

95% C. L. allowed regions in the plane $(\kappa - \tilde{\kappa})$ for the process $\gamma\gamma \to \tau^+\tau^-$ for the first, second and third stage of operation of the CLIC, where a fixed center-of-mass energies of $\sqrt{s} = 380, 1500, 3000\,GeV$ is assumed with luminosities of $\mathcal{L} = 10, 100, 500\,fb^{-1}$, $\mathcal{L} = 100, 500, 1500\,fb^{-1}$ and $\mathcal{L} = 100, 500, 3000\,fb^{-1}$, respectively, and considering systematic uncertainties of $\delta_{sys} = 0\%, 3\%, 5\,\%$ [14, 74], they are displayed in Figs. 8-10. For a complementary description on the uncertainties we suggest the reader consult Refs. [70, 75].

The achievable precision in the determination of the anomalous magnetic moment $\tilde{a}_\tau$ and the electric dipole moment $\tilde{d}_\tau$ are summarized in Figs. 11-14 and Tables IV-VI and are compared with experimental results of earlier studios for a linear collider as published by the BELLE, DELPHI, L3 and OPAL Collaboration [14–18]. Our results show that the two-photon process $\gamma\gamma \to \tau^+\tau^-$ at the CLIC improve the sensitivity bounds on anomalous electromagnetic dipole moments of tau-lepton with respect to the existing experimental bounds (see Table I) by two orders of magnitude. Our best bounds obtained on $\tilde{a}_\tau$ and $\tilde{d}_\tau$ are $-0.00015 \le \tilde{a}_\tau \le 0.00017$ and $|\tilde{d}_\tau(ecm)| = 9.040 \times 10^{-19}$, respectively, as shown in Tables IV-VI.

C. $\gamma\gamma \to \tau^+\tau^-\gamma$ cross section

Experimentally, the processes that involving single-photon in the final state $(\tau^+\tau^-\gamma)$ can potentially distinguish from background associated with the process under consideration. Furthermore, the anomalous $\tau^+\tau^-\gamma$ coupling can be analyzed through the process $e^+e^- \to \tau^+\tau^-$ at the linear colliders. This process receives contributions from both anomalous $\tau^+\tau^-\gamma$ and $\tau^+\tau^-Z$ couplings. However, the processes $\gamma\gamma \to \tau^+\tau^-$ and $\gamma\gamma \to \tau^+\tau^-\gamma$ isolate $\tau^+\tau^-\gamma$ coupling which provides the possibility to analyze the $\tau^+\tau^-\gamma$ coupling separately from the $\tau^+\tau^-Z$ coupling. In general, anomalous values of $\tilde{a}_\tau$ and $\tilde{d}_\tau$ tend to increase the cross section for the process $\gamma\gamma \to \tau^+\tau^-\gamma$, especially for photons with high energy which are well isolated from the decay products of the taus [15]. Additionally, the single-photon in the final state

13

TABLE IV: Sensitivity on the $\tilde{a}_\tau$ magnetic moment and the $\tilde{d}_\tau$ electric dipole moment for $\sqrt{s} = 380\,GeV$ and $\mathcal{L} = 10, 50, 100, 300, 500\,fb^{-1}$ at 95% C.L. through the process $\gamma\gamma \to \tau\bar{\tau}$.

$\sqrt{s} = 380\,GeV,$		95% C.L.	
$\mathcal{L}\,(fb^{-1})$	δ_{sys}	$\tilde{a}_\tau$	$|\tilde{d}_\tau(ecm)|$
10	0%	[-0.00232; 0.00095]	1.071×10^{-17}
10	3%	[-0.00603; 0.00464]	2.999×10^{-17}
10	5%	[-0.00756; 0.00616]	3.826×10^{-17}
50	0%	[-0.00189; 0.00052]	8.813×10^{-18}
50	3%	[-0.00603; 0.00464]	2.998×10^{-17}
50	5%	[-0.00756; 0.00616]	3.825×10^{-17}
100	0%	[-0.00176; 0.00039]	8.298×10^{-18}
100	3%	[-0.00603; 0.00464]	2.998×10^{-17}
100	5%	[-0.00756; 0.00616]	3.825×10^{-17}
300	0%	[-0.00161; 0.00025]	7.737×10^{-18}
300	3%	[-0.00603; 0.00464]	2.998×10^{-17}
300	5%	[-0.00756; 0.00616]	3.825×10^{-17}
500	0%	[-0.00156; 0.00019]	7.556×10^{-18}
500	3%	[-0.00603; 0.00464]	2.997×10^{-17}
500	5%	[-0.00756; 0.00616]	3.825×10^{-17}

has the advantage of being identifiable with high efficiency and purity.

They may also provide a clear signal in the detector for new physics, for new phenomena such as the dipole moments of fermions. Also, the selection criteria used for the analysis allow the search for events having the characteristics of single-photon.

We now turn attention to the process $\gamma\gamma \to \tau^+\tau^-\gamma$ at future e^+e^- collider. On the technical side, for the calculation of the total cross section of $\gamma\gamma \to \tau^+\tau^-\gamma$, the analytical expression for the amplitude square is quite lengthy so we do not present it here. Instead, we present numerical fit functions for the total cross sections with respect to center-of-mass energy and in terms of the parameters κ and $\tilde{\kappa}$. Furthermore, in the case of the process

14

TABLE V: Sensitivity on the $\tilde{a}_\tau$ magnetic moment and the $\tilde{d}_\tau$ electric dipole moment for $\sqrt{s} = 1.5\,TeV$ and $\mathcal{L} = 100, 300, 500, 1000, 1500\, fb^{-1}$ at 95% C.L. through the process $\gamma\gamma \to \tau\bar{\tau}$.

$\mathcal{L}\,(fb^{-1})$	δ_{sys}	$\tilde{a}_\tau$	$|\tilde{d}_\tau(ecm)|$
$\sqrt{s} = 1.5\,TeV,$ \quad 95% C.L.			
100	0%	[-0.00061; 0.00041]	2.796×10^{-18}
100	3%	[-0.00209; 0.00189]	1.109×10^{-17}
100	5%	[-0.00267; 0.00247]	1.428×10^{-17}
300	0%	[-0.00049; 0.00029]	2.1226×10^{-18}
300	3%	[-0.00209; 0.00189]	1.108×10^{-17}
300	5%	[-0.00267; 0.00247]	1.428×10^{-17}
500	0%	[-0.00044; 0.00025]	1.867×10^{-18}
500	3%	[-0.00209; 0.00189]	1.108×10^{-17}
500	5%	[-0.00267; 0.00247]	1.428×10^{-17}
1000	0%	[-0.00039; 0.00019]	1.567×10^{-18}
1000	3%	[-0.00209; 0.00189]	1.108×10^{-17}
1000	5%	[-0.00267; 0.00247]	1.427×10^{-17}
1500	0%	[-0.00037; 0.00017]	1.415×10^{-18}
1500	3%	[-0.00209; 0.00189]	1.108×10^{-17}
1500	5%	[-0.00267; 0.00247]	1.427×10^{-17}

$\gamma\gamma \to \tau^+\tau^-\gamma$, we apply the following kinematic cuts to reduce the background and to maximize the signal sensitivity:

$$
\begin{aligned}
p_t^\gamma &> 20\,GeV, \quad |\eta^\gamma| < 2.5, \\
p_t^{\tau,\bar{\tau}} &> 20\,GeV, \quad |\eta^{\tau,\bar{\tau}}| < 2.5, \\
\Delta R(\tau, \gamma) &> 0.4, \\
\Delta R(\tau, \bar{\tau}) &> 0.4, \\
\Delta R(\bar{\tau}, \gamma) &> 0.4,
\end{aligned}
\tag{24}
$$

for the photon transverse momentum p_t^γ, the photon pseudorapidity η^γ which reduces the

TABLE VI: Sensitivity on the $\tilde{a}_\tau$ magnetic moment and the $\tilde{d}_\tau$ electric dipole moment for $\sqrt{s} = 3\,TeV$ and $\mathcal{L} = 100, 500, 1000, 2000, 3000\,fb^{-1}$ at 95% C.L. through the process $\gamma\gamma \to \tau\bar{\tau}$.

$\mathcal{L}\,(fb^{-1})$	δ_{sys}	$\tilde{a}_\tau$	$|\tilde{d}_\tau(ecm)|$
$\sqrt{s} = 3\,TeV$, 95% C.L.			
100	0%	[-0.00037; 0.00039]	2.116×10^{-18}
100	3%	[-0.00114; 0.00115]	6.342×10^{-18}
100	5%	[-0.00147; 0.00148]	8.153×10^{-18}
500	0%	[-0.00025; 0.00026]	1.415×10^{-18}
500	3%	[-0.00114; 0.00115]	6.335×10^{-18}
500	5%	[-0.00147; 0.00148]	8.153×10^{-18}
1000	0%	[-0.00020; 0.00022]	1.190×10^{-18}
1000	3%	[-0.00114; 0.00115]	6.334×10^{-18}
1000	5%	[-0.00147; 0.00148]	8.153×10^{-18}
2000	0%	[-0.00017; 0.00018]	1.000×10^{-18}
2000	3%	[-0.00114; 0.00115]	6.334×10^{-18}
2000	5%	[-0.00147; 0.00148]	8.153×10^{-18}
3000	0%	[-0.00015; 0.00017]	9.040×10^{-19}
3000	3%	[-0.00114; 0.00115]	6.334×10^{-18}
3000	5%	[-0.00147; 0.00148]	8.153×10^{-18}

contamination from other particles misidentified as photon, the tau transverse momentum $p_t^{\tau,\bar{\tau}}$ for the final state particles, the tau pseudorapidity η^τ which reduces the contamination from other particles misidentified as tau and $\Delta R(\tau, \gamma)$, $\Delta R(\tau, \bar{\tau})$ and $\Delta R(\bar{\tau}, \gamma)$ are the separation of the final state particles. In conclusion, by using these cuts given in Eq. (24) in our manuscript we have taken into account isolation criteria to optimize the signal to the particles of the $\tau^+\tau^-\gamma$ final state. The cases considered are:

- For $\sqrt{s} = 380\,GeV$.

$$\begin{aligned}
\sigma(\kappa) &= \big[(3.22 \times 10^7)\kappa^6 + (4.08 \times 10^4)\kappa^5 + (3.36 \times 10^5)\kappa^4 + (1.87 \times 10^3)\kappa^3 \\
&\quad + (1.24 \times 10^3)\kappa^2 + (0.515)\kappa + 0.21\big](pb),
\end{aligned}$$
(25)

$$\sigma(\tilde{\kappa}) = \big[(3.22 \times 10^7)\tilde{\kappa}^6 + (3.43 \times 10^5)\tilde{\kappa}^4 + (1.24 \times 10^3)\tilde{\kappa}^2 + 0.21\big](pb).$$
(26)

- For $\sqrt{s} = 1500\,GeV$.

$$\begin{aligned}
\sigma(\kappa) &= \big[(8.29 \times 10^9)\kappa^6 + (8.65 \times 10^6)\kappa^5 + (1.15 \times 10^7)\kappa^4 + (3.90 \times 10^3)\kappa^3 \\
&\quad + (3.74 \times 10^3)\kappa^2 + (0.31)\kappa + 0.116\big](pb),
\end{aligned}$$
(27)

$$\sigma(\tilde{\kappa}) = \big[(8.29 \times 10^9)\tilde{\kappa}^6 + (1.15 \times 10^7)\tilde{\kappa}^4 + (3.74 \times 10^3)\tilde{\kappa}^2 + 0.116\big](pb).$$
(28)

- For $\sqrt{s} = 3000\,GeV$.

$$\begin{aligned}
\sigma(\kappa) &= \big[(1.33 \times 10^{11})\kappa^6 + (4.63 \times 10^7)\kappa^5 + (5.58 \times 10^7)\kappa^4 + (1.46 \times 10^3)\kappa^3 \\
&\quad + (4.92 \times 10^3)\kappa^2 + (0.47)\kappa + 0.052\big](pb),
\end{aligned}$$
(29)

$$\sigma(\tilde{\kappa}) = \big[(1.33 \times 10^{11})\tilde{\kappa}^6 + (5.58 \times 10^7)\tilde{\kappa}^4 + (4.92 \times 10^3)\tilde{\kappa}^2 + 0.052\big](pb).$$
(30)

It is worth mentioning that in the equations for the total cross section (25)-(30), the coefficients of $\kappa(\tilde{\kappa})$ given the anomalous contribution, while the independent terms of $\kappa(\tilde{\kappa})$ correspond to the cross section at $\kappa = \tilde{\kappa} = 0$ and represents the SM cross section magnitude.

D.   Bounds on $\tilde{a}_\tau$ and $\tilde{d}_\tau$ through $\gamma\gamma \to \tau^+\tau^-\gamma$ at the CLIC

Next, we focus our attention on the numerical calculation for the total cross section and for the electromagnetic dipole moments of the tau-lepton. To carry out our objective, we start with Eqs. (25)-(30) and adopting the collider parameters of $\sqrt{s} = 380, 1500, 3000\,GeV$ for the center-of-mass energy and $\mathcal{L} = 10, 50, 100, 300, 500, 1000, 1500, 2000, 3000\,fb^{-1}$ for the integrated luminosity of data. In addition, we apply kinematic cuts given by Eq. (24) to optimize the signal and to reduce the background, and an important part of our study

is the inclusion of systematic uncertainties of $\delta_{sys} = 0\%, 3\%, 5\%$. Our calculations yield the following results.

Figs. 15 and 16 present the results for the total cross section for the $\gamma\gamma \to \tau^+\tau^-\gamma$ scenario, where the total cross sections for $\sigma(\gamma\gamma \to \tau^+\tau^-\gamma)$ vs $\kappa(\tilde{\kappa})$ are shown for $\sqrt{s} = 380, 1500, 3000\, GeV$, respectively. In both cases, the dependence of the total cross section $\sigma(\sqrt{s}, \kappa, \tilde{\kappa})$ presents a clear dependence with respect to $\sqrt{s}$, as well as with the anomalous parameters κ and $\tilde{\kappa}$. For case of comparison the total cross section for $\gamma\gamma \to \tau^+\tau^-$ is major by a factor of 10 compared to the $\gamma\gamma \to \tau^+\tau^-\gamma$ scenario. To visualize the effects of κ and $\tilde{\kappa}$ on the total cross section $\sigma_{\gamma\gamma\to\tau^+\tau^-\gamma}(\sqrt{s}, \kappa, \tilde{\kappa})$ we display Figs. 17-19.

The contours plots on $\tilde{\kappa}$ and $\tilde{\kappa}$ at the 95% C.L., are obtained using Eqs. (25)-(30), these are shown in Figs. 20-22 for integrate luminosities of $\mathcal{L} = 10, 100, 500, 1500, 3000\, fb^{-1}$ with $\sqrt{s} = 380, 1500, 3000\, GeV$, respectively. The improvement in the sensitivity on $\tilde{\kappa}$ and $\tilde{\kappa}$ is obtained using high energy and high luminosity as is immediately apparent from these figures.

The estimated sensitivity of the CLIC for $\tilde{a}_\tau(\tilde{d}_\tau)$ at 95% C.L., as well as for different center-of-mass energies, luminosities and systematic errors is illustrated in Figs. 23-26. The sensitivity is 1-2 orders of magnitude better for all couplings than that expected at the the current colliders (see Table I) and the potential to disentangle $\tilde{a}_\tau$ and $\tilde{d}_\tau$ improves at larger $\sqrt{s}$ and $\mathcal{L}$.

To conclude with our set of results, we present, through Tables VII-IX, the bounds corresponding to the magnetic and electric dipole moments of the τ-lepton, via the $\gamma\gamma \to \tau^+\tau^-\gamma$ mode. The center-of-mass energies and luminosities assumed are $\sqrt{s} = 380, 1500, 3000$ and $\mathcal{L} = 10, 50, 100, 300, 500, 1000, 1500, 2000, 3000\, fb^{-1}$, respectively, and only one anomalous coupling $\tilde{a}_\tau(\tilde{d}_\tau)$ was varied at a time to bound its value. In the present study, the sensitivities are based on the systematic errors of $\delta_{sys} = 0\%, 3\%, 5\%$ and our best bounds are: $-0.00033 \leq \tilde{a}_\tau \leq 0.00023$ and $|\tilde{d}_\tau(ecm)| = 1.546 \times 10^{-18}$, respectively. These bounds are weaker by an order of magnitude than those corresponding to the $\gamma\gamma \to \tau^+\tau^-$ mode (see Subsection B, Tables IV-VI). But stronger than those reported by BELLE, DELPHI, L3 and OPAL Collaborations (see Table 1).

TABLE VII: Sensitivity on the $\tilde{a}_\tau$ magnetic moment and the $\tilde{d}_\tau$ electric dipole moment for $\sqrt{s} = 380\,GeV$ and $\mathcal{L} = 10, 50, 100, 300, 500\,fb^{-1}$ at 95% C.L. through the process $\gamma\gamma \to \tau\bar{\tau}\gamma$.

	$\sqrt{s} = 380\,GeV,$	95% C.L.	
$\mathcal{L}\,(fb^{-1})$	δ_{sys}	$\tilde{a}_\tau$	$|\tilde{d}_\tau(ecm)|$
10	0%	[-0.00351; 0.00308]	1.813×10^{-17}
10	3%	[-0.00375; 0.00332]	1.977×10^{-17}
10	5%	[-0.00449; 0.00405]	2.385×10^{-17}
50	0%	[-0.00245; 0.00203]	1.213×10^{-17}
50	3%	[-0.00348; 0.00305]	1.829×10^{-17}
50	5%	[-0.00435; 0.00391]	2.306×10^{-17}
100	0%	[-0.00211; 0.00169]	1.020×10^{-17}
100	3%	[-0.00344; 0.00301]	1.807×10^{-17}
100	5%	[-0.00433; 0.00389]	2.296×10^{-17}
300	0%	[-0.00169; 0.00127]	7.758×10^{-18}
300	3%	[-0.00342; 0.00299]	1.792×10^{-17}
300	5%	[-0.00432; 0.00388]	2.289×10^{-17}
500	0%	[-0.00153; 0.00111]	6.828×10^{-18}
500	3%	[-0.00341; 0.00298]	1.789×10^{-17}
500	5%	[-0.00432; 0.00388]	2.288×10^{-17}

III. CONCLUSIONS

In this paper we have presented a complete study of the total cross section as well as of the anomalous magnetic and electric dipole moments of the tau-lepton in the scenarios $\gamma\gamma \to \tau^+\tau^-$ and $\gamma\gamma \to \tau^+\tau^-\gamma$ at the CLIC. To investigate these scenarios, we have considered a set of parameters $\tilde{a}_\tau$ and $\tilde{d}_\tau$ for both processes, as well as the parameters $\sqrt{s}$ and $\mathcal{L}$ of the collider. Furthermore, for each of these scenarios we considered a set of cuts appropriate given by Eqs. (12) and (24) to reduce the background and to optimize the signal sensitivity to the particles of the $\tau^+\tau^-(\tau^+\tau^-\gamma)$ final state.

Overall, our study shows that the scenario $\gamma\gamma \to \tau^+\tau^-$ with two-tau in the final state, is

19

TABLE VIII: Sensitivity on the $\tilde{a}_\tau$ magnetic moment and the $\tilde{d}_\tau$ electric dipole moment for $\sqrt{s} = 1.5\,TeV$ and $\mathcal{L} = 100, 300, 500, 1000, 1500\,fb^{-1}$ at 95% C.L. through the process $\gamma\gamma \to \tau\bar{\tau}\gamma$.

$\mathcal{L}\,(fb^{-1})$	δ_{sys}	$\sqrt{s} = 1.5\,TeV$, 95% C.L. $\tilde{a}_\tau$	$\|\tilde{d}_\tau(ecm)\|$
100	0%	[-0.00096; 0.00088]	5.121×10^{-18}
100	3%	[-0.00142; 0.00134]	7.695×10^{-18}
100	5%	[-0.00179; 0.00171]	9.756×10^{-18}
300	0%	[-0.00074; 0.00066]	3.926×10^{-18}
300	3%	[-0.00140; 0.00132]	7.582×10^{-18}
300	5%	[-0.00178; 0.00170]	9.702×10^{-18}
500	0%	[-0.00066; 0.00058]	3.475×10^{-18}
500	3%	[-0.00140; 0.00131]	7.559×10^{-18}
500	5%	[-0.00178; 0.00170]	9.691×10^{-18}
1000	0%	[-0.00057; 0.00049]	2.952×10^{-18}
1000	3%	[-0.00139; 0.00131]	7.541×10^{-18}
1000	5%	[-0.00178; 0.00170]	9.683×10^{-18}
1500	0%	[-0.00052; 0.00044]	2.688×10^{-18}
1500	3%	[-0.00139; 0.00131]	7.535×10^{-18}
1500	5%	[-0.00178; 0.00170]	9.680×10^{-18}

more representative and projects a better sensitivity in both, the total cross section and in the bounds on the electromagnetic dipole moments in comparison with the process $\gamma\gamma \to \tau^+\tau^-\gamma$ in the entire range of center-of-mass energies and luminosities of the future CLIC. Another important aspect in our study that is worth mentioning to distinguish the sensitivity in our results is the incorporation of the systematic uncertainties of $\delta_{sys} = 0, 3, 5\,\%$.

In summary, we have shown that the two-photon $\gamma\gamma \to \tau^+\tau^-$ and $\gamma\gamma \to \tau^+\tau^-\gamma$ processes at the CLIC leads to a remarkable improvement in the existing experimental bounds on the $\tilde{a}_\tau$ and $\tilde{d}_\tau$. In the case of the scenario $\gamma\gamma \to \tau^+\tau^-$ we get a significant improvement of the order of magnitude of 3.466×10^2 for the upper bound and of 0.764×10^2 for the lower

TABLE IX: Sensitivity on the $\tilde{a}_\tau$ magnetic moment and the $\tilde{d}_\tau$ electric dipole moment for $\sqrt{s} = 3\,TeV$ and $\mathcal{L} = 100, 500, 1000, 20000, 3000\ fb^{-1}$ at 95% C.L. through the process $\gamma\gamma \to \tau\bar{\tau}\gamma$.

$\sqrt{s} = 3\,TeV,$	95% C.L.		
$\mathcal{L}\,(fb^{-1})$	δ_{sys}	$\tilde{a}_\tau$	$|\tilde{d}_\tau(ecm)|$
100	0%	[-0.00070; 0.00060]	3.612×10^{-18}
100	3%	[-0.00087; 0.00078]	4.591×10^{-18}
100	5%	[-0.00108; 0.00098]	5.740×10^{-18}
500	0%	[-0.00048; 0.00039]	2.418×10^{-18}
500	3%	[-0.00084; 0.00075]	4.422×10^{-18}
500	5%	[-0.00106; 0.00097]	5.658×10^{-18}
1000	0%	[-0.00041; 0.00032]	2.034×10^{-18}
1000	3%	[-0.00084; 0.00074]	4.399×10^{-18}
1000	5%	[-0.00106; 0.00097]	5.647×10^{-18}
2000	0%	[-0.00035; 0.00026]	1.711×10^{-18}
2000	3%	[-0.00083; 0.00074]	4.388×10^{-18}
2000	5%	[-0.00106; 0.00097]	5.642×10^{-18}
3000	0%	[-0.00033; 0.00023]	1.546×10^{-18}
3000	3%	[-0.00083; 0.00074]	4.384×10^{-18}
3000	5%	[-0.00106; 0.00097]	5.640×10^{-18}

bound in comparison with the results published by the DELPHI and BELLE Collaborations for the reaction $e^+e^- \to \tau^+\tau^-$ [14, 17]. In the case of the scenario $\gamma\gamma \to \tau^+\tau^-\gamma$ the improvement is of the order of 2.060×10^2 and 2.826×10^2 for the upper and lower bounds, respectively, in comparison with the reported by the L3 and OPAL Collaborations for the process $e^+e^- \to \tau^+\tau^-\gamma$ [15, 16], as shown in Table I. Our results indicate and shown that the processes $\gamma\gamma \to \tau^+\tau^-$ and $\gamma\gamma \to \tau^+\tau^-\gamma$ are more suitable for probing the electromagnetic dipole moments of the τ-lepton in the future e^+e^- linear colliders such as the CLIC at the

$\gamma\gamma$ mode.

Acknowledgments

---

[1] S. L. Glashow, *Nucl. Phys.* **22**, 579 (1961).

[2] S. Weinberg, *Phys. Rev. Lett.* **19**, 1264 (1967).

[3] A. Salam, in *Elementary Particle Theory*, Ed. N. Svartholm (Almquist and Wiskell, Stockholm, 1968) 367.

[4] D. Hanneke, S. Fogwell, and G. Gabrielse, *Phys. Rev. Lett.* **100**, 120801 (2008).

[5] G. Bennett, *et al.*, *Phys. Rev.* **D73**, 072003 (2006), hep-ex/0602035.

[6] C. Patrignani, *et al.*, [Particle Data Group], *Chin. Phys.* **C40**, 100001 (2016).

[7] S. Eidelman and M. Passera, *Mod. Phys. Lett.* **A22**, 159 (2007).

[8] M. A. Samuel, G. Li and R. Mendel R, 1991 *Phys. Rev. Lett.* **67**, 668 (1991); M. A. Samuel, G. Li and R. Mendel, 1992 *Phys. Rev. Lett.* **69**, 995 (1992) (erratum).

[9] F. Hamzeh and N. F. Nasrallah, 1996 *Phys. Lett.* **B373**, 211 (1996).

[10] S. M. Barr and W. Marciano, *in CP Violation*, ed. C. Jarlskog (World Scientific, Singapore, 1990).

[11] J. H. Christenson, J. W. Cronin, V. L. Fitch, and R. Turlay, *Phys. Rev. Lett.* **13**, 138 (1964).

[12] K. Abe, *et al.*, *Phys. Rev. Lett.* **87**, 091802 (2001).

[13] R. Aaij, *et al.* [LHCb Collaboration], *J. High Energy Phys.* **07** (2014) 041.

[14] J. Abdallah, *et. al.*, [DELPHI Collaboration], *Eur. Phys. J.* **C35**, 159 (2004).

[15] M. Acciarri, *et. al.*, [L3 Collaboration], *Phys. Lett.* **B434**, 169 (1998).

[16] K. Ackerstaff, *et. al.*, [OPAL Collaboration], *Phys. Lett.* **B431**, 188 (1998).

[17] K. Inami, *et al.*, [BELLE Collaboration], *Phys. Lett.* **B551**, 16 (2003).

[18] H. Albrecht, *et al.*, [ARGUS Collaboration], *Phys. Lett.* **B485**, 37 (2000).

[19] J. A. Grifols and A. Méndez, *Phys. Lett.* **B255**, 611 (1991); Erratum **ibid. B259**, 512 (1991).

[20] R. Escribano and E. Massó, *Phys. Lett.* **B395**, 369 (1997).

[21] G. A. González-Sprinberg, *et al.*, *Nucl. Phys.* **B582** 3 (2000).

[22] D. J. Silverman, G. L. Shaw, 83 *Phys. Rev.* **D27**, 1196 (1983).

[23] F. del Aguila, M. Sher 90 *Phys. Lett.* **B252**, 116 (1990).

[24] E. O. Iltan, *Eur. Phys. J.* **C44**, 411 (2005).

[25] B. Dutta, R. N. Mohapatra, *Phys. Rev.* **D68**, 113008 (2003).

[26] E. Iltan, *Phys. Rev.* **D64**, 013013 (2001).

[27] E. Iltan, *JHEP* **065**, 0305 (2003).

[28] E. Iltan, *JHEP 0404*, 018 (2004).

[29] A. Gutiérrez-Rodríguez, M. A. Hernández-Ruíz and L.N. Luis-Noriega, *Mod. Phys. Lett.* **A19**, 2227 (2004).

[30] A. Gutiérrez-Rodríguez, M. A. Hernández-Ruíz and M. A. Pérez, *Int. J. Mod. Phys.* **A22**, 3493 (2007).

[31] A. Gutiérrez-Rodríguez, *Mod. Phys. Lett.* **A25**, 703 (2010).

[32] A. Gutiérrez-Rodríguez, M. A. Hernández-Ruíz, C. P. Castañeda-Almanza, *J. Phys.* **G40**, 035001 (2013).

[33] M. Köksal, S. C. Inan, A. A. Billur, M. K. Bahar, Y. Özgüven, arXiv:1711.02405 [hep-ph].

[34] Y. Özgüven, S. C. Inan, A. A. Billur, M. Köksal, M. K. Bahar, *Nucl. Phys.* **B923**, 475 (2017).

[35] A. A. Billur, M. Köksal, *Phys. Rev. D89*, 037301 (2014).

[36] L. Tabares, O. A. Sampayo, *Phys. Rev.* **D65**, 053012 (2002).

[37] S. Eidelman, D. Epifanov, M. Fael, L. Mercolli, M. Passera, *JHEP* **1603**, 140 (2016).

[38] Iftah Galon, Arvind Rajaraman, Tim M. P. Tait, *JHEP* **1612**, 111 (2016).

[39] M. A. Arroyo-Ureña, *et al.*, *Eur. Phys. J.* C77, 227 (2017).

[40] M. A. Arroyo-Ureña, *et al.*, Int. J. Mod. Phys. A32, 1750195 (2017).

[41] Xin Chen, *et al.*, arXiv:1803.00501.

[42] Antonio Pich, Prog. Part. Nucl. Phys. 75, 41-85 (2014).

[43] S. Atag and E. Gurkanli, *JHEP* **1606**, 118 (2016).

[44] Lucas Taylor, *Nucl. Phys. Proc. Suppl.* **76**, 237 (1999).

[45] A. Gutiérrez-Rodríguez, M. A. Hernández-Ruíz, L. N. Luis-Noriega, *J. Phys. Conf. Ser.* **37**, 25 (2006).

[46] M. Passera, *Nucl. Phys. Proc. Suppl.* **169**, 213 (2007).

[47] M. Passera, *Phys. Rev.* **D75**, 013002 (2007).

[48] J. Bernabeu, G. A. González-Sprinberg, J. Papavassiliou, J. Vidal, *Nucl. Phys.* **B790**, 160 (2008).

[49] A. Gutiérrez-Rodríguez, *et al.*, *Nucl. Phys. Proc. Suppl.* **253-255**, 202 (2014).

[50] W. Bernreuther, O. Nachtmann, P. Overmann, *Phys. Rev.* **D48**, 78 (1993).

[51] L. Linssen, *et al.*, *CLIC Conceptual Design Report: Physics and Detectors at CLIC*, CERN-2012-003 (2012).

[52] E. Accomando, *et al.* [CLIC Physisc Working Group Collaboration], arXiv: hep-ph/0412251, CERN-2004-005.

[53] H. Abramowicz, *et al.*, *The CLIC Detector and Physics Study*, arXiv:1307.5288 [hep-ex].

[54] D. Dannheim, P. Lebrun, L. Linssen et al., arXiv: 1208.1402 [hep-ex].

[55] A. Gutiérrez-Rodríguez, M. Koksal and A. A. Billur, *Phys. Rev.* **D91**, 093008 (2015).

[56] M. Köksal, S. C. Inan, *Adv. High Energy Phys.* **2014**, 315826 (2014).

[57] M. Köksal *Mod. Phys. Lett.* **A29**, 1450184 (2014).

[58] C. Giunti and A. Studenkin, *Rev. Mod. Phys.* **87**, 531(2015).

[59] B. Grzadkowski, M. Iskrzynski, M. Misiak, and J. Rosiek, *JHEP* **10**, 085 (2010); [arXiv:1008.4884].

[60] M. Fael, *Electromagnetic dipole moments of fermions*, PhD. Thesis, (2014).

[61] S. Eidelman, D. Epifanov, M. Fael, L. Mercolli and M. Passera, *JHEP* **1603**, 140 (2016).

[62] A. Belyaev, N. D. Christensen and A. Pukhov, *Comput. Phys. Commun.* **184**, 1729 (2013).

[63] Martin L. Perl, *et al.*, *Phys. Rev. Lett.* **35**, 1489 (1975).

[64] Martin L. Perl, *Rep. Prog. Phys.* **55**, 653 (1992).

[65] G. Bagliesi, *J. Phys. Conf. Ser.* **119**, 032005 (2008).

[66] I. Sahin and M. Koksal, *JHEP* **03**, 100 (2011).

[67] H. Abramowicz, *et al.*, *CLIC Detector and Physics Study Collaboration*, arXiv:1307.5288.

[68] M. Aicheler, *et al.*, (editors), *A Multi-TeV Linear Collider based on CLIC Technology: CLIC Conceptual Design Report*, JAI-2012-001, KEK Report 2012-1, PSI-12-01, SLAC-R-

985, https://edms.cern.ch/document/1234244/.

[69] L. Linssen, *et al.*, (editors),*Physics and Detectors at CLIC: CLIC Conceptual Design Report*, 2012, ANL-HEP-TR-12-01, CERN-2012-003, DESY 12-008, KEK Report 2011-7, arXiv:1202.5940.

[70] S. Atag and A. A. Billur, *JHEP* **11**, 060 (2010).

[71] A. Kalinowski, *Nucl. Phys. B Proc. Suppl.* **189**, 305 (2009).

[72] S. Lai, *et al.*, [ATLAS Collaboration], ATL-PHYS-PROC-2009-126.

[73] T. H. Tran, V. Balagura, V. Boudry, J. C. Brient, H. Videau, *Eur. Phys. J.* **C76**, 468 (2016).

[74] P. Achard, *et al.*, [L3 Collaboration], *Phys. Lett.* **B585**, 53 (1998).

[75] S. Chatrchyan, *et al.,* [CMS Collaboration], *JHEP* **1201**, 052 (2012).
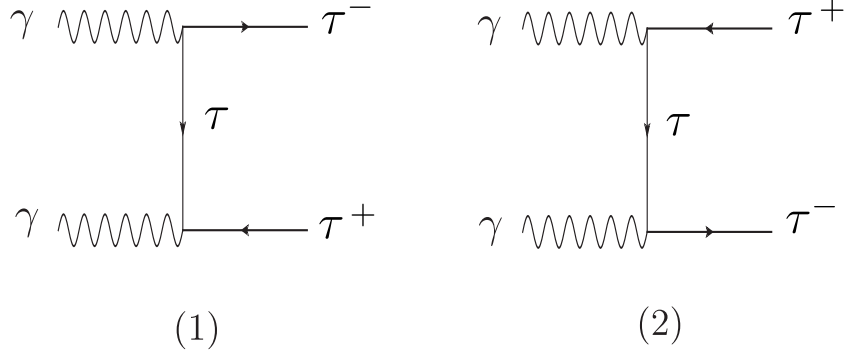
FIG. 1:   The Feynman diagrams for the process $\gamma\gamma \to \tau^+\tau^-$.
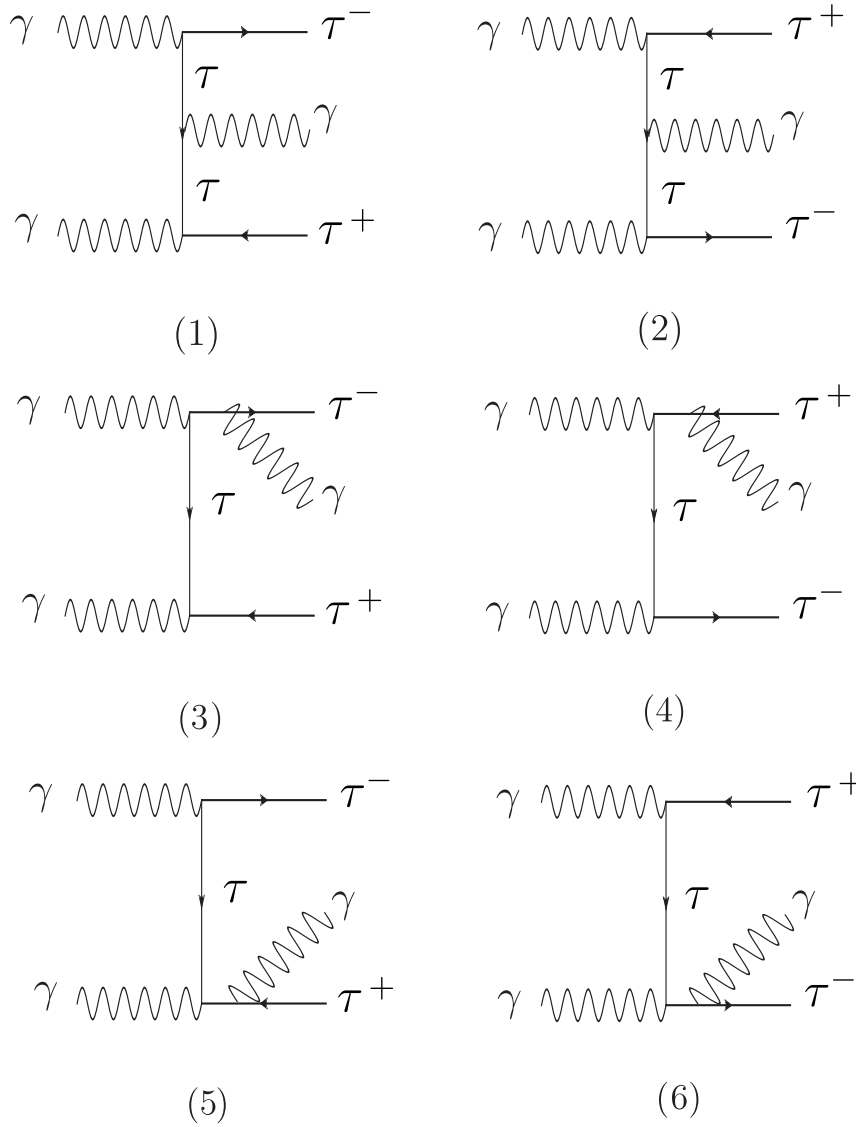
FIG. 2:   The Feynman diagrams for the process $\gamma\gamma \to \tau^+\tau^-\gamma$.
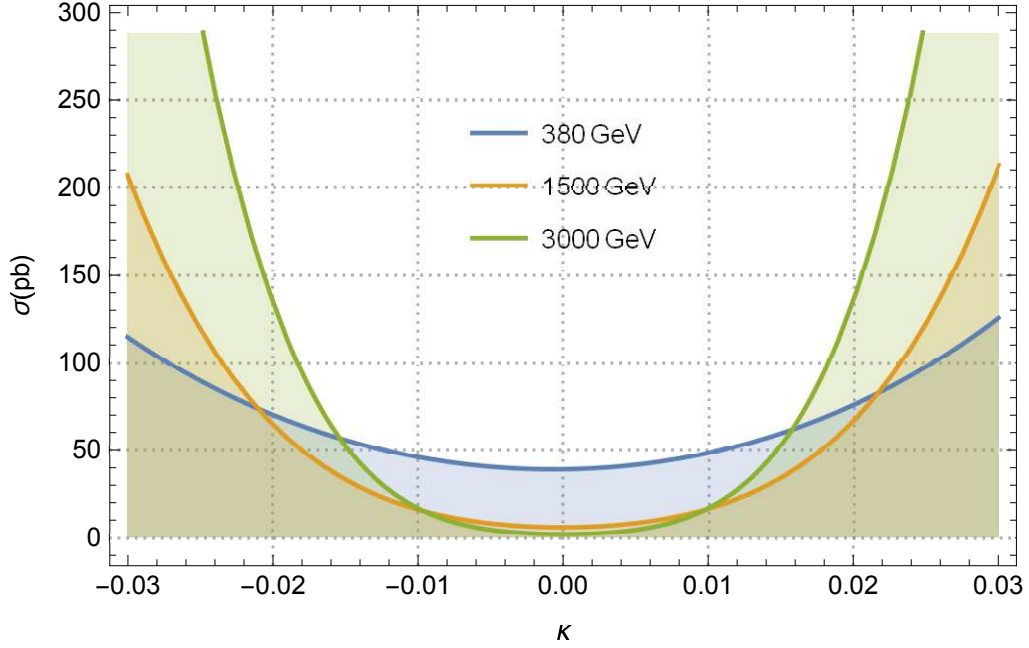
FIG. 3: The total cross sections of the process $\gamma\gamma \to \tau^+\tau^-$ as a function of κ for center-of-mass energies of $\sqrt{s} = 380, 1500, 3000\ GeV$.
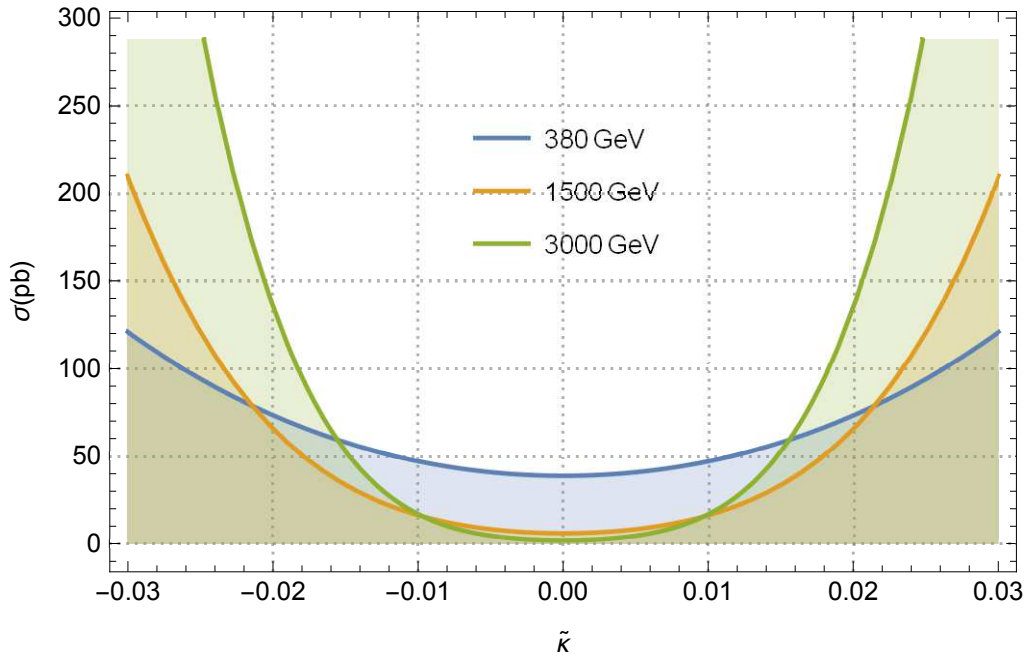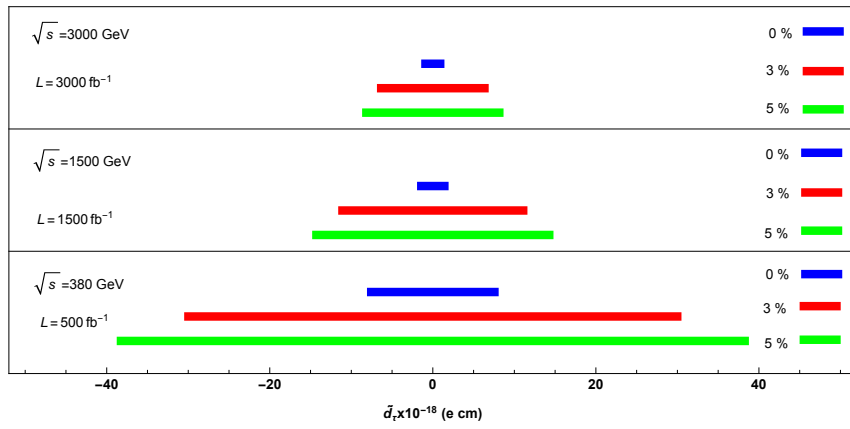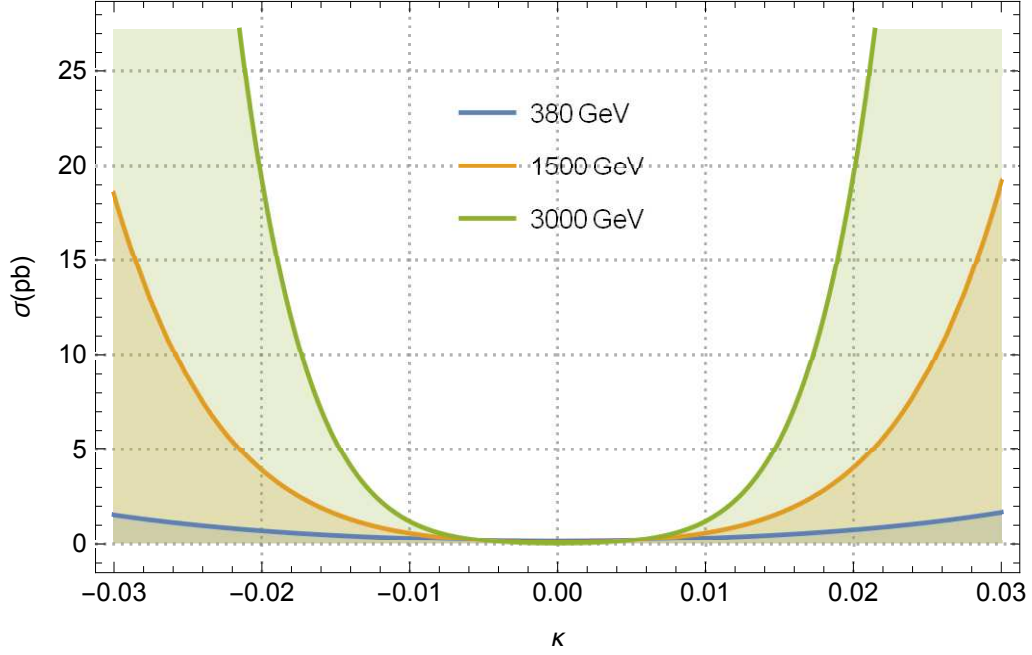

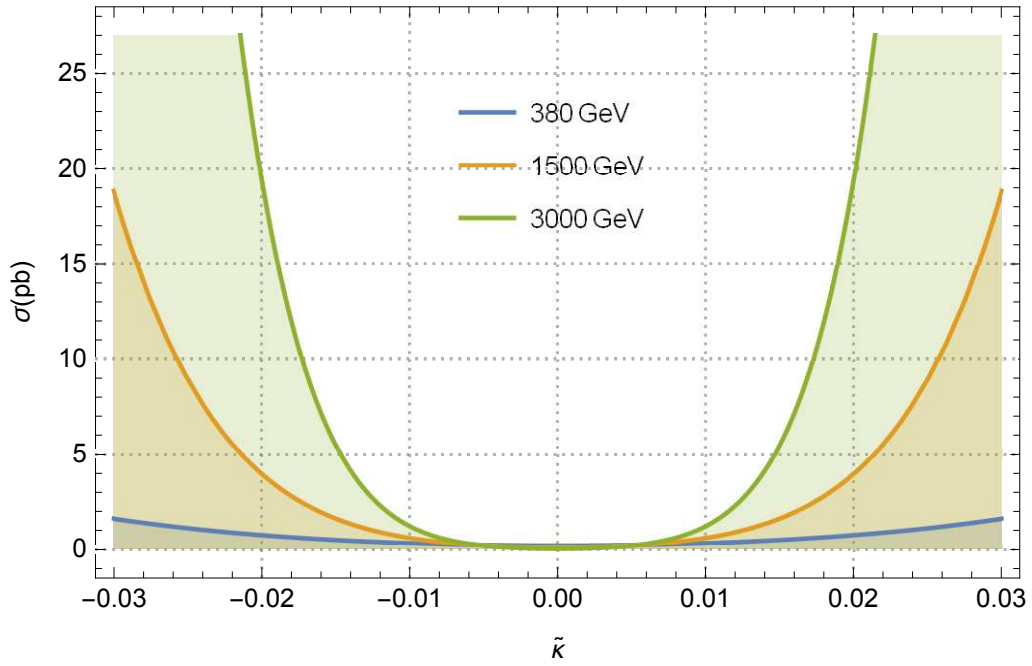FIG. 4: Same as in Fig. 3, but for $\tilde{\kappa}$.
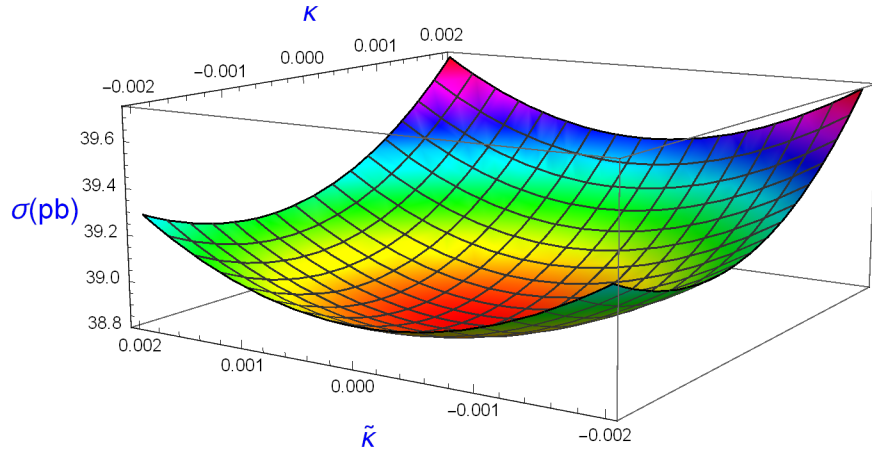
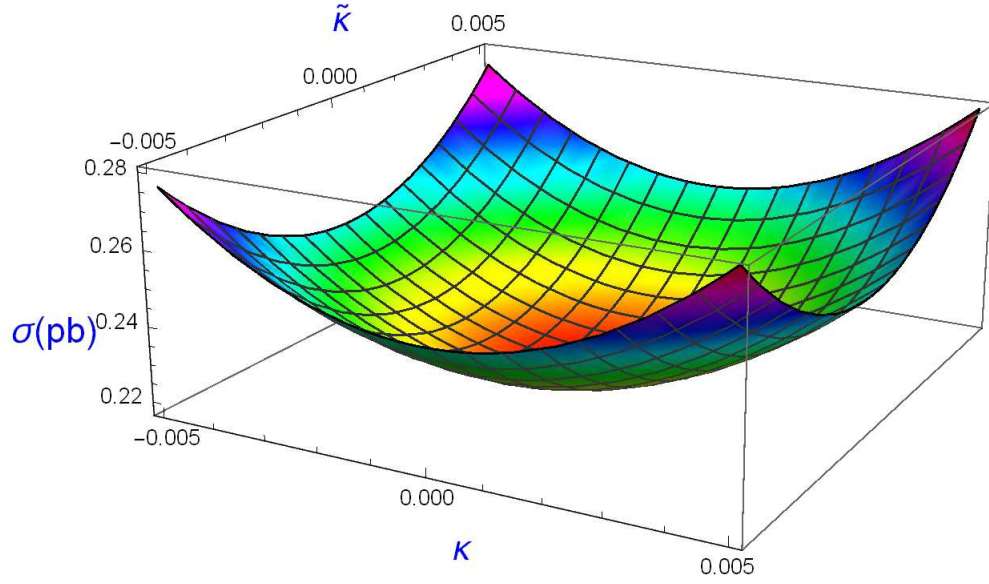FIG. 5: The total cross sections of the process $\gamma\gamma \to \tau^+\tau^-$ as a function of κ and $\tilde{\kappa}$ for center-of-mass energy of $\sqrt{s} = 380\,GeV$.
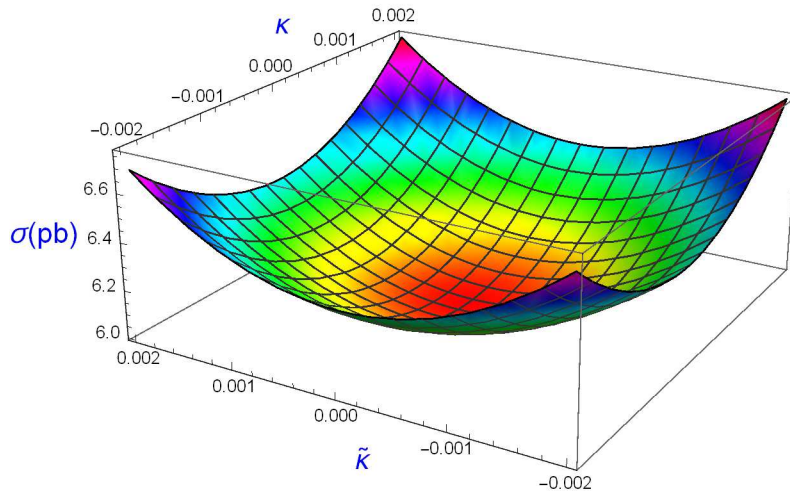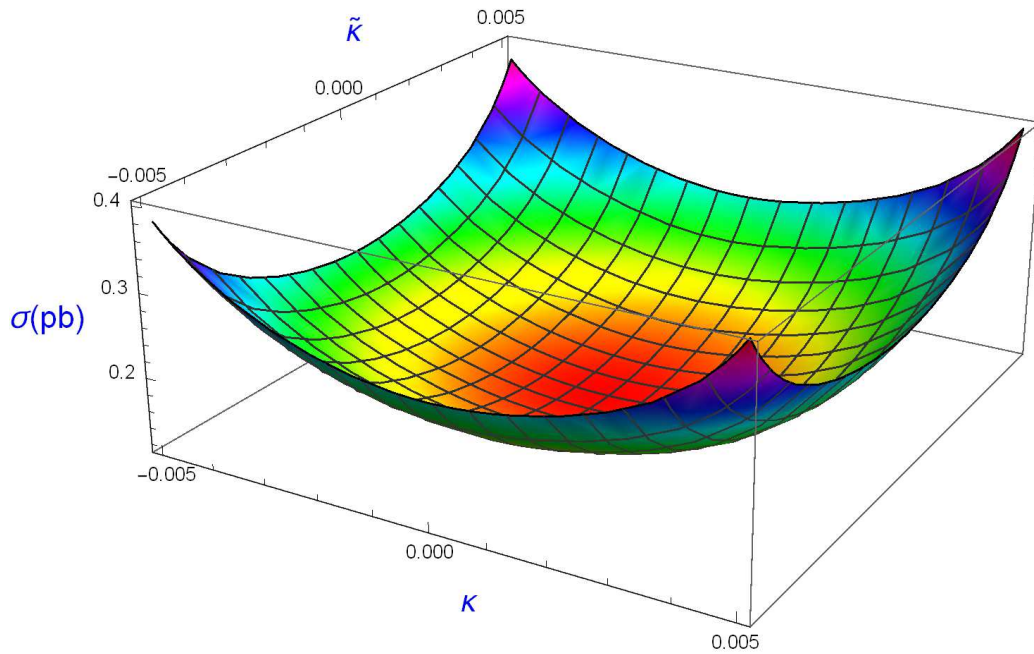

FIG. 6: Same as in Fig. 5, but for $\sqrt{s} = 1500\,GeV$.
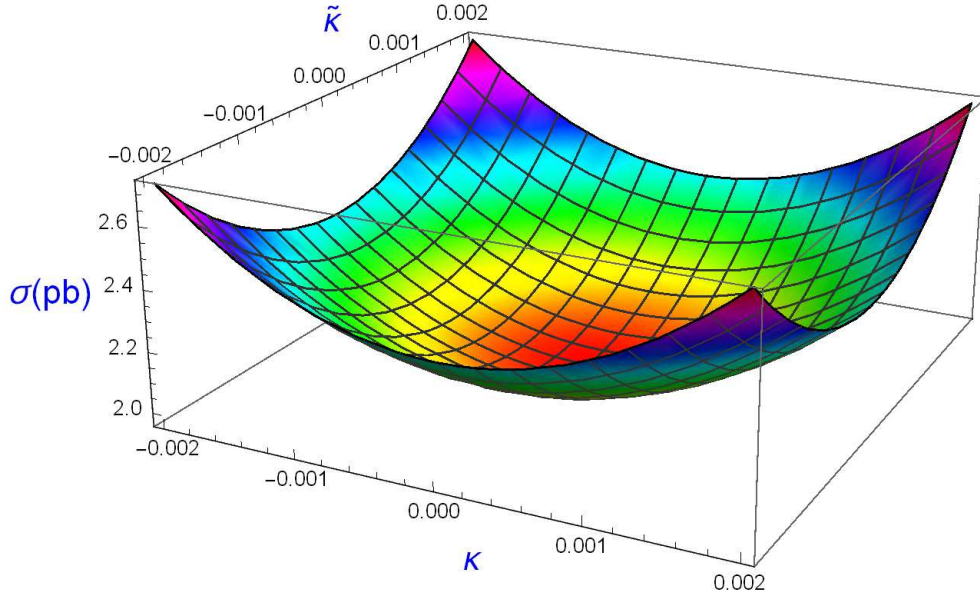
FIG. 7: Same as in Fig. 5, but for $\sqrt{s} = 3000 \, GeV$.
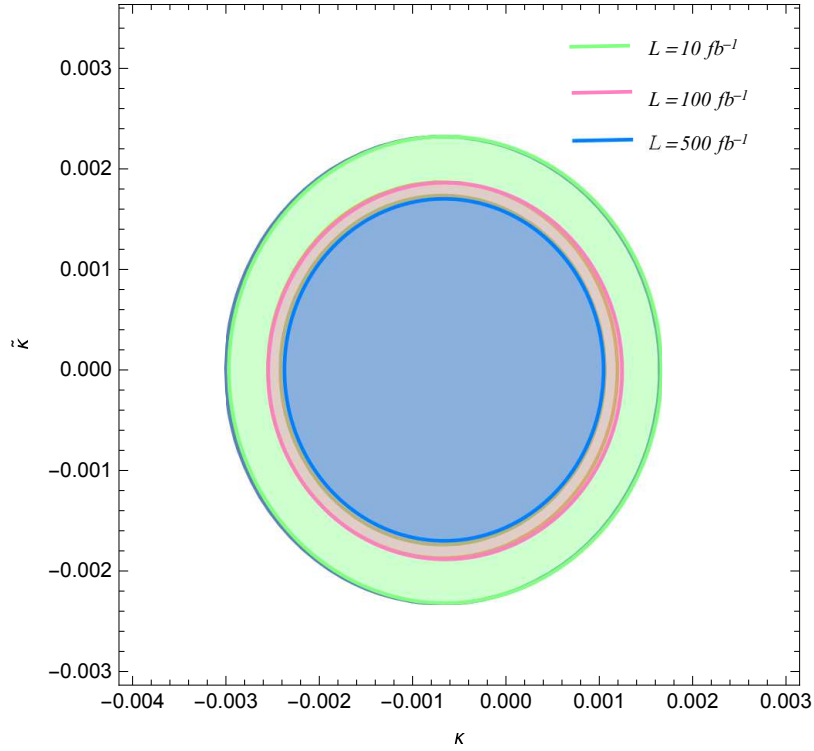
FIG. 8: Bounds contours at the $95\% \, C.L.$ in the $(\kappa - \tilde{\kappa})$ plane for the process $\gamma\gamma \to \tau^+\tau^-$ with the $\mathcal{L} = 10, 100, 500 \, fb^{-1}$ and for center-of-mass energy of $\sqrt{s} = 380 \, GeV$.

29
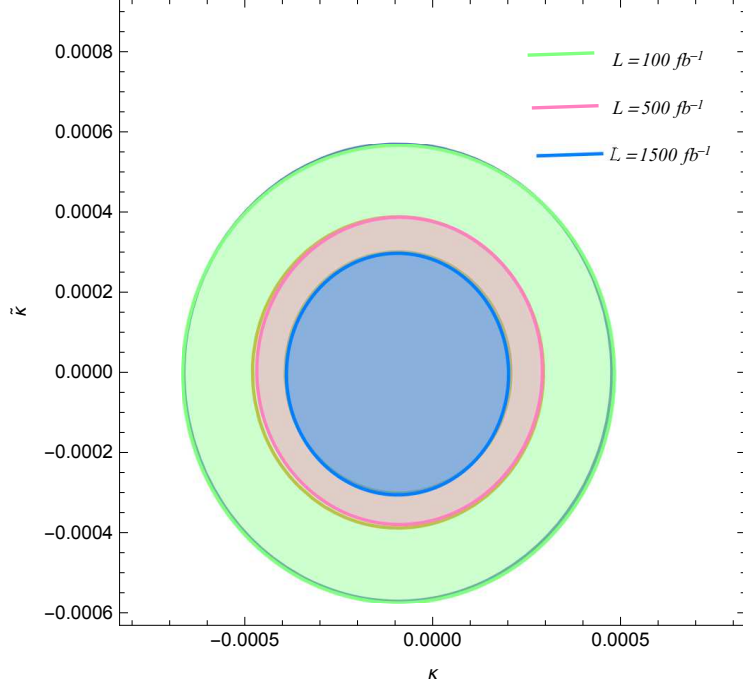
FIG. 9: Same as in Fig. 8, but for $\mathcal{L} = 100, 500, 1500\, fb^{-1}$ and for center-of-mass energy of $\sqrt{s} = 1500\, GeV$.
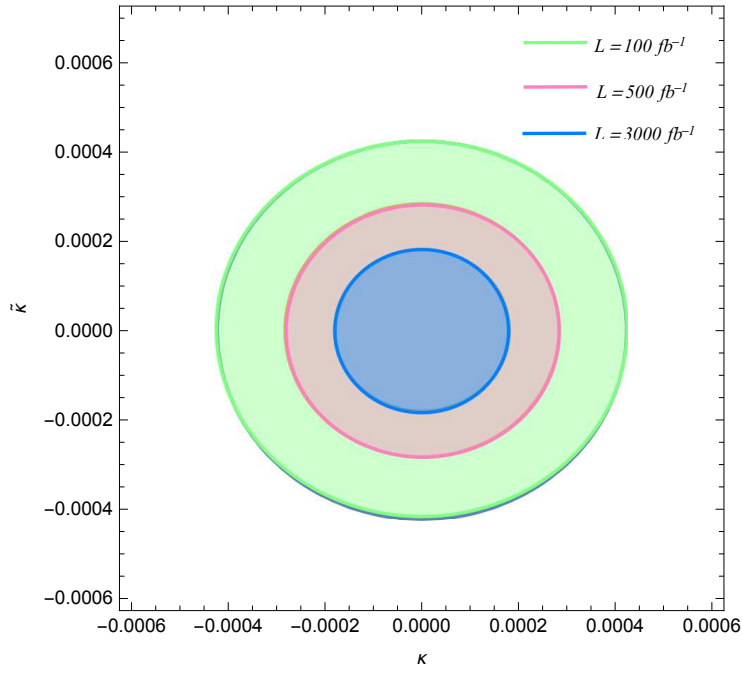
FIG. 10: Same as in Fig. 8, but for $\mathcal{L} = 100, 500, 3000\, fb^{-1}$ and for center-of-mass energy of $\sqrt{s} = 3000\, GeV$.
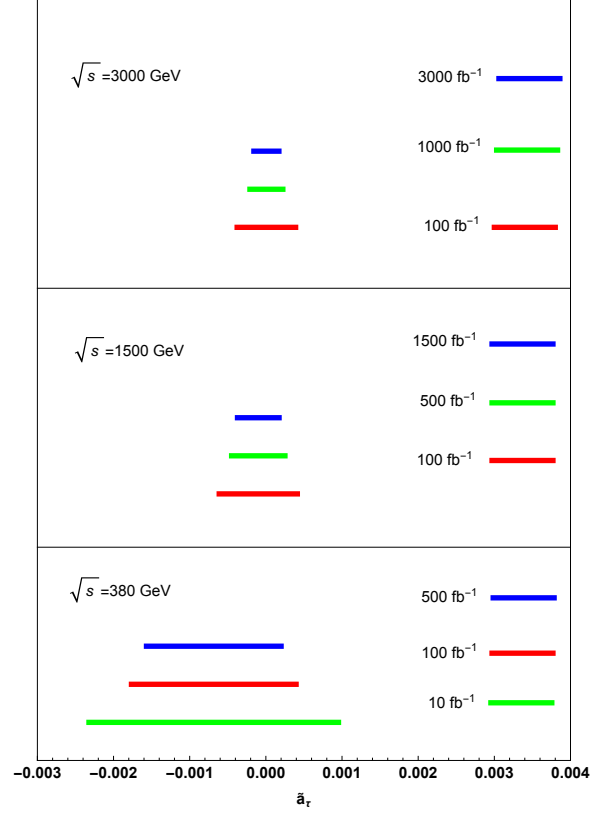
FIG. 11: Comparison of precisions on $\tilde{a}_\tau$ in the process $\gamma\gamma \to \tau^+\tau^-$ expected at the CLIC. We assume luminosities of, Top panel: $\mathcal{L} = 100, 1000, 3000\, fb^{-1}$ and $\sqrt{s} = 3000\, GeV$. Central panel: $\mathcal{L} = 100, 500, 1500\, fb^{-1}$ and $\sqrt{s} = 1500\, GeV$. Bottom panel: $\mathcal{L} = 10, 100, 500\, fb^{-1}$ and $\sqrt{s} = 380\, GeV$.
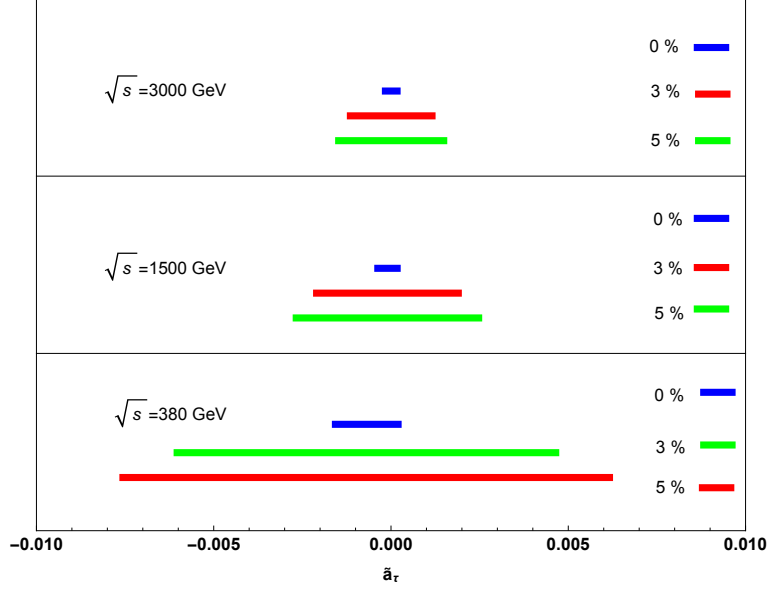
FIG. 12: Same as in Fig. 11, but for, Top panel: $\delta_{sys} = 0, 3, 5\,\%$ with $\mathcal{L} = 3000\ fb^{-1}$ and $\sqrt{s} = 3000\ GeV$. Central panel: $\delta_{sys} = 0, 3, 5\,\%$ with $\mathcal{L} = 1500\ fb^{-1}$ and $\sqrt{s} = 1500\ GeV$. Bottom panel: $\delta_{sys} = 0, 3, 5\,\%$ with $\mathcal{L} = 500\ fb^{-1}$ and $\sqrt{s} = 380\ GeV$.
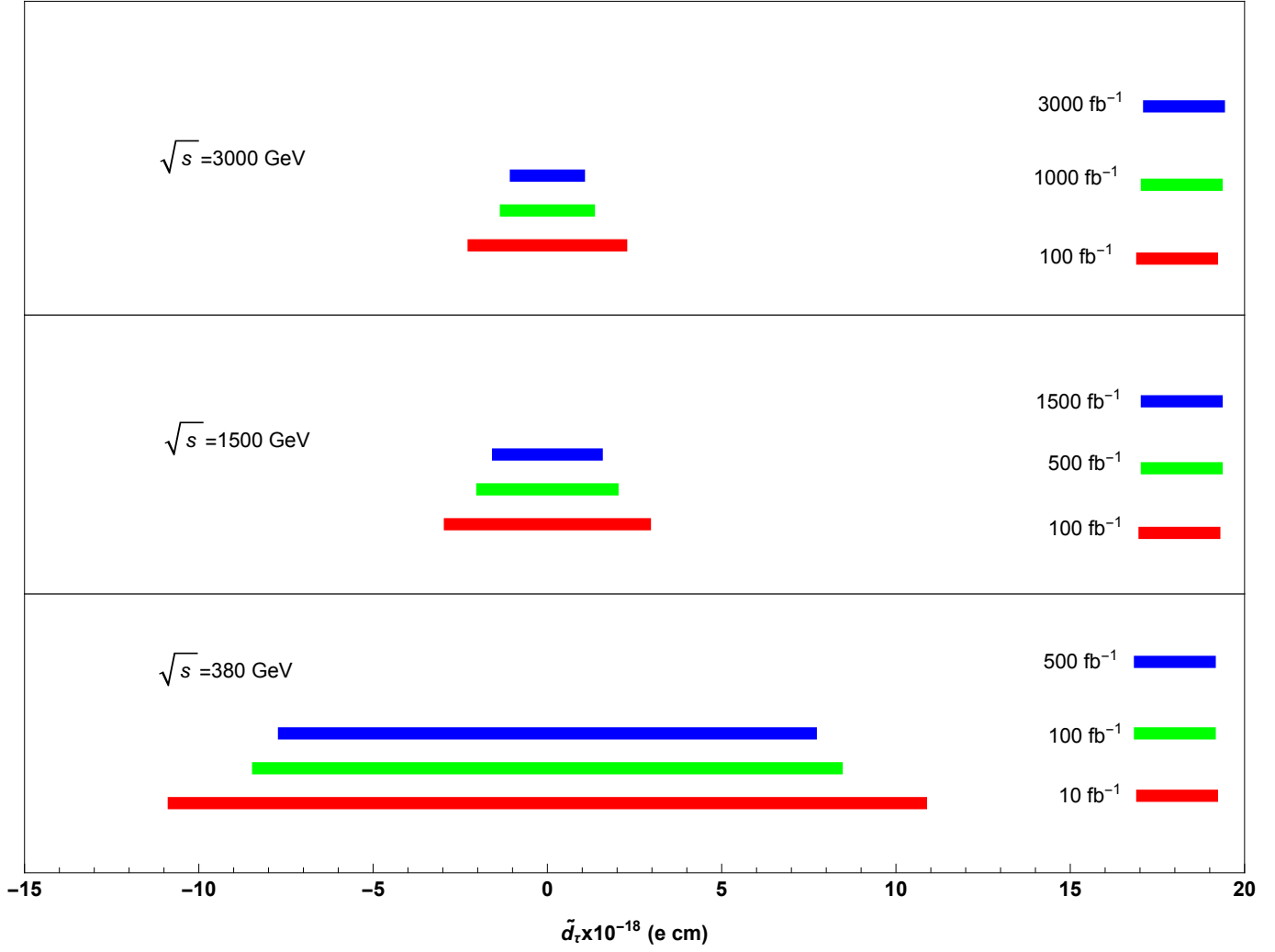
FIG. 13:   Same as in Fig. 11, but for $\tilde{d}_\tau$.

FIG. 14:   Same as in Fig. 12, but for $\tilde{d}_\tau$.

33

FIG. 15: The total cross sections of the process $\gamma\gamma \to \tau^+\tau^-\gamma$ as a function of κ for center-of-mass energies of $\sqrt{s} = 380, 1500, 3000~GeV$.

FIG. 16: Same as in Fig. 15, but for $\tilde{\kappa}$.

FIG. 17:   The total cross sections of the process $\gamma\gamma \rightarrow \tau^+\tau^-\gamma$ as a function of κ and $\tilde{\kappa}$ for center-of-mass energy of $\sqrt{s} = 380\,GeV$.

FIG. 18:   Same as in Fig. 17, but for $\sqrt{s} = 1500\,GeV$.
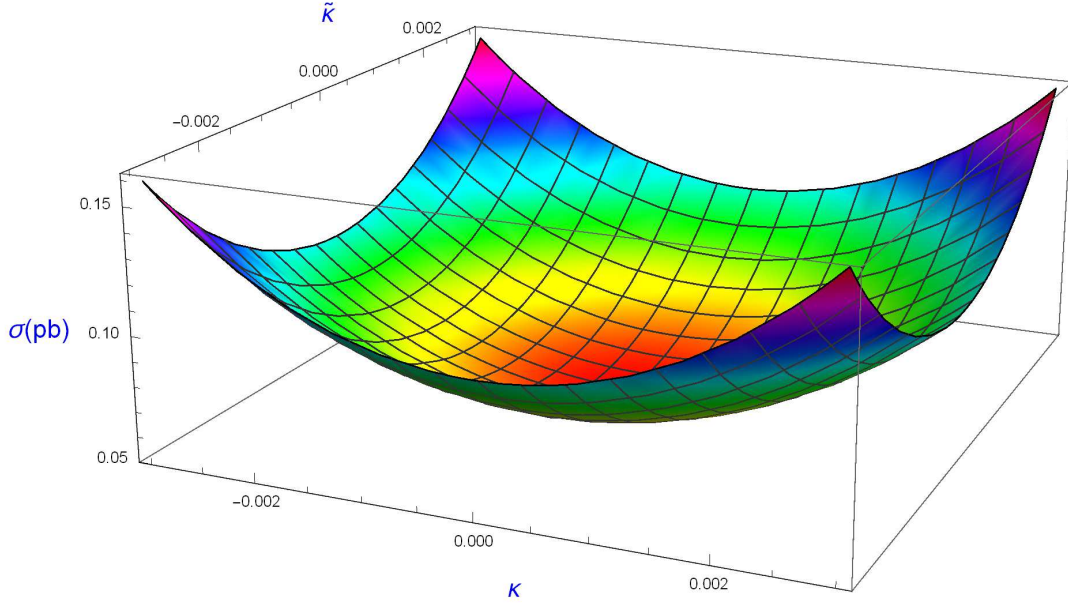
FIG. 19: Same as in Fig. 17, but for $\sqrt{s} = 3000\,GeV$.
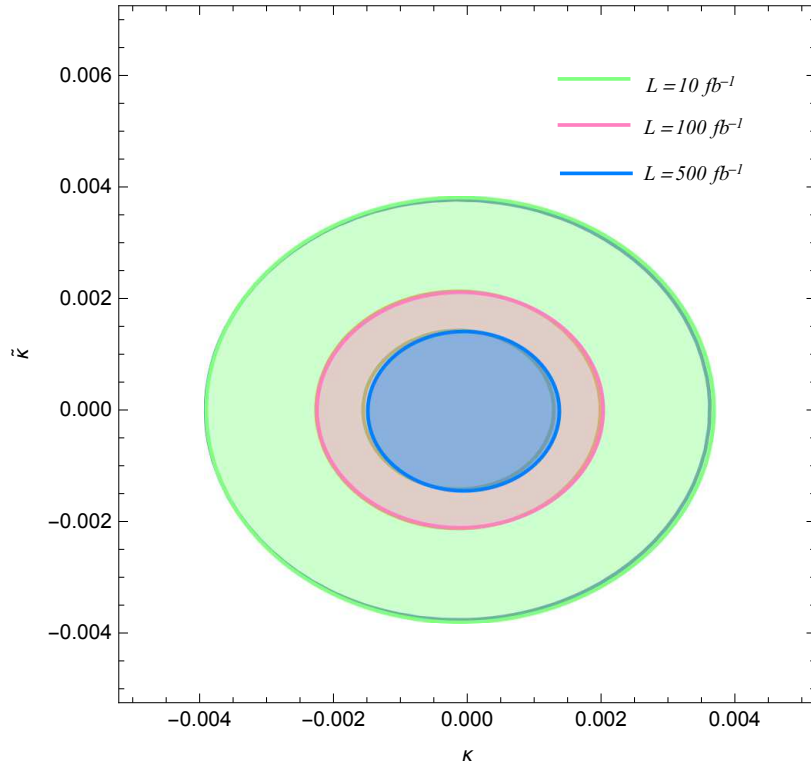
FIG. 20: Bounds contours at the $95\%\ C.L.$ in the $(\kappa - \tilde{\kappa})$ plane for the process $\gamma\gamma \to \tau^+\tau^-\gamma$ with the $\mathcal{L} = 10, 100, 500\ fb^{-1}$ and for center-of-mass energy of $\sqrt{s} = 380\,GeV$.
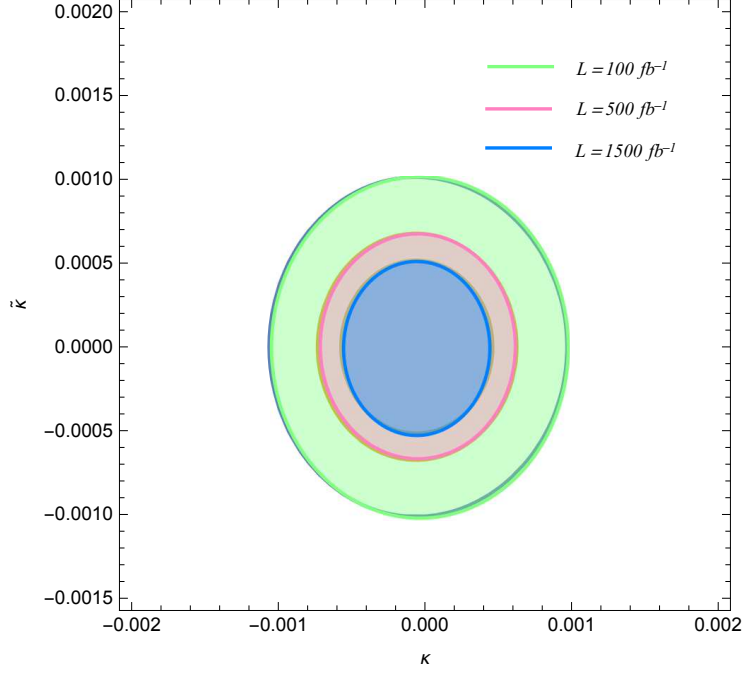
FIG. 21: Same as in Fig. 20, but for $\mathcal{L} = 100, 500, 1500 \, fb^{-1}$ and for center-of-mass energy of $\sqrt{s} = 1500 \, GeV$.
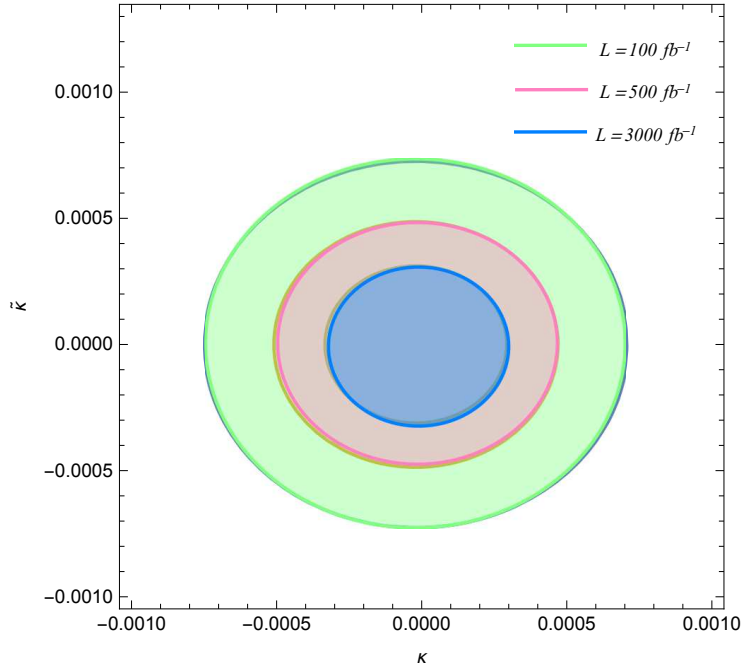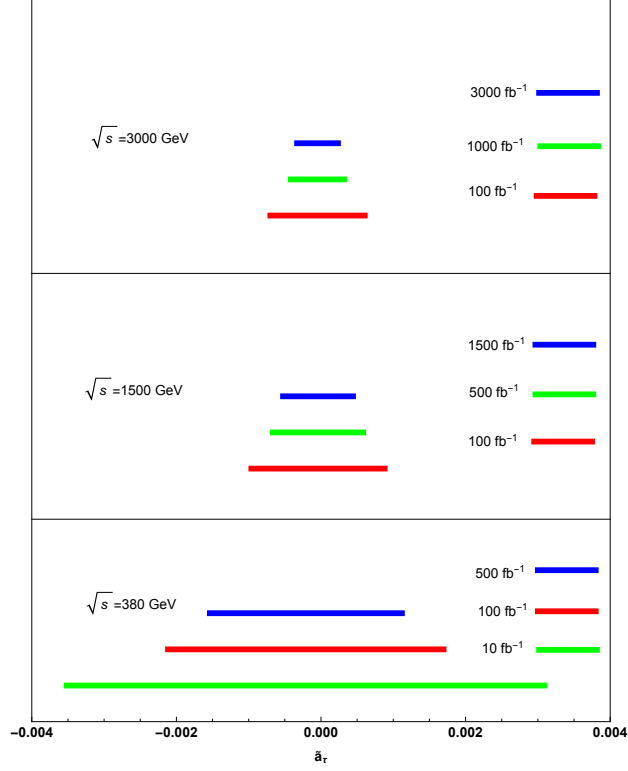

FIG. 22: Same as in Fig. 20, but for $\mathcal{L} = 100, 500, 3000 \, fb^{-1}$ and for center-of-mass energy of $\sqrt{s} = 3000 \, GeV$.

37

FIG. 23: Comparison of precisions on $\tilde{a}_\tau$ in the process $\gamma\gamma \to \tau^+\tau^-\gamma$ expected at the CLIC. We assume luminosities of, Top panel: $\mathcal{L} = 100, 1000, 3000\ fb^{-1}$ and $\sqrt{s} = 3000\ GeV$. Central panel: $\mathcal{L} = 100, 500, 1500\ fb^{-1}$ and $\sqrt{s} = 1500\ GeV$. Bottom panel: $\mathcal{L} = 10, 100, 500\ fb^{-1}$ and $\sqrt{s} = 380\ GeV$.
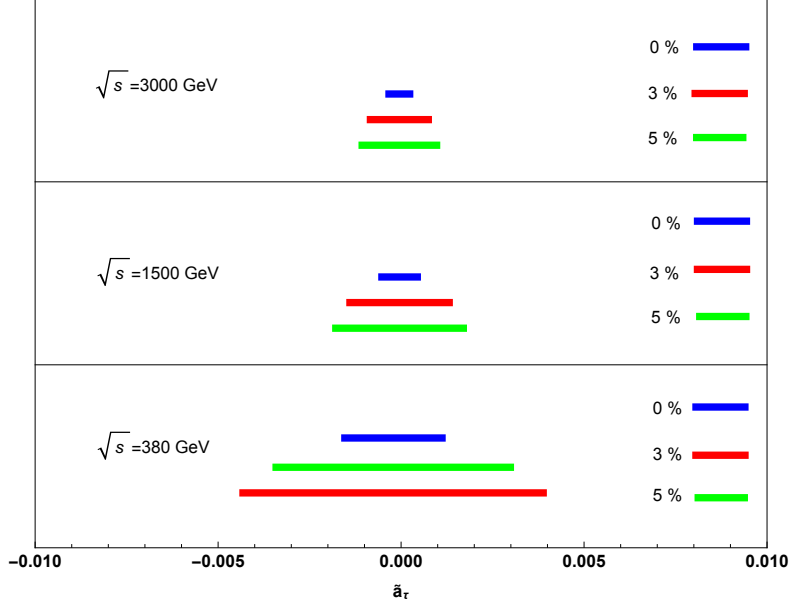
FIG. 24: Same as in Fig. 23, but for, Top panel: $\delta_{sys} = 0, 3, 5\,\%$ with $\mathcal{L} = 3000\,fb^{-1}$ and $\sqrt{s} = 3000\,GeV$. Central panel: $\delta_{sys} = 0, 3, 5\,\%$ with $\mathcal{L} = 1500\,fb^{-1}$ and $\sqrt{s} = 1500\,GeV$. Bottom panel: $\delta_{sys} = 0, 3, 5\,\%$ with $\mathcal{L} = 500\,fb^{-1}$ and $\sqrt{s} = 380\,GeV$.
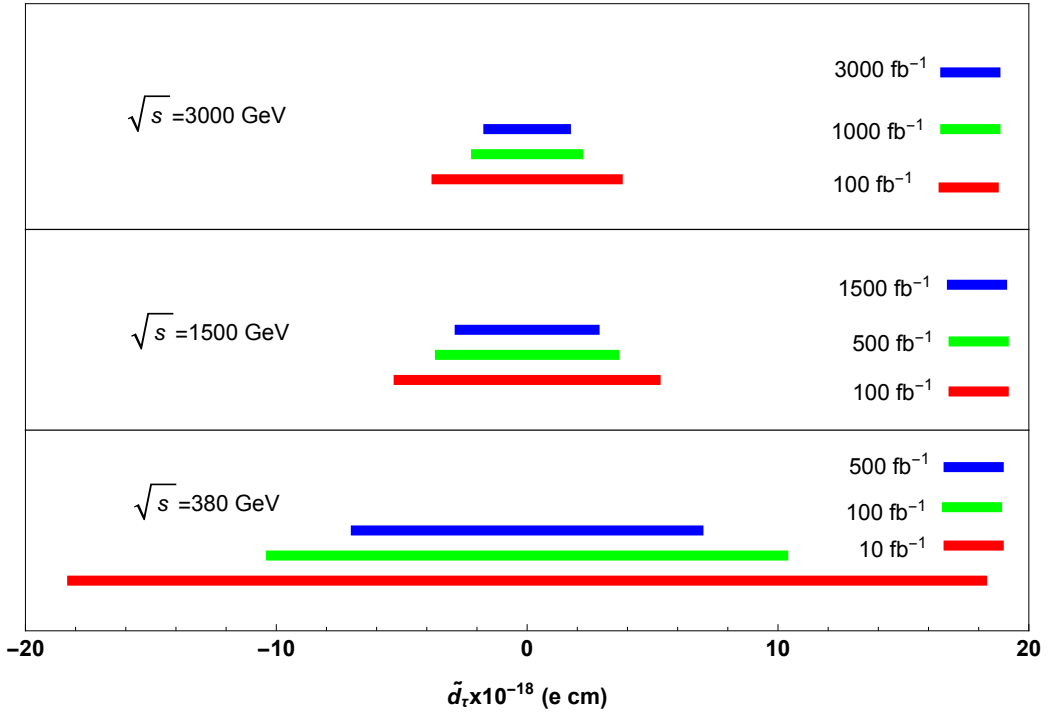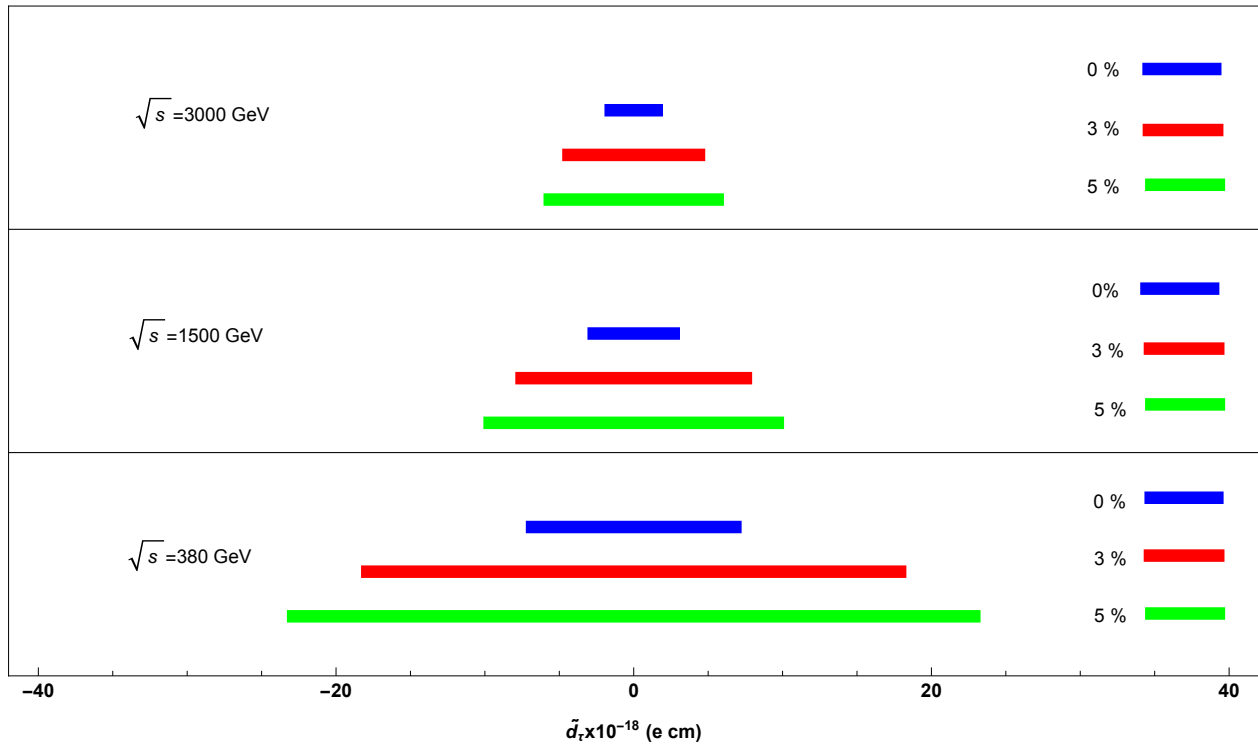

FIG. 25: Same as in Fig. 23, but for $\tilde{d}_\tau$.

FIG. 26: Same as in Fig. 24, but for $\tilde{d}_\tau$.